Plasma 2
Lecture 9: Alfvén Waves

APPH E6102y
Columbia University

Outline

- Ch. 6.5 Magnetohydrodynamic Waves
- Bounded plasma waves: shear Alfvén wave resonance

6.5 Magnetohydrodynamic Waves

$$\frac{\partial \rho_{\mathrm{m1}}}{\partial t} + \rho_{\mathrm{m0}} \boldsymbol{\nabla} \cdot \mathbf{U}_1 = 0, \tag{6.5.1}$$

$$\rho_{\mathrm{m0}} \frac{\partial \mathbf{U}_1}{\partial t} = \frac{1}{\mu_0} (\boldsymbol{\nabla} \times \mathbf{B}_1) \times \mathbf{B}_0 - \boldsymbol{\nabla} P_1, \tag{6.5.2}$$

$$\frac{\partial \mathbf{B}_1}{\partial t} = \boldsymbol{\nabla} \times (\mathbf{U}_1 \times \mathbf{B}_0), \tag{6.5.3}$$

$$P_1 = \gamma \left(\frac{P_0}{\rho_{\mathrm{m0}}} \right) \rho_{\mathrm{m1}}. \tag{6.5.4}$$

$$V_{\mathrm{S}}^2 = \gamma \frac{P_0}{\rho_{\mathrm{m0}}} = \frac{\gamma \kappa T_0}{m}, \tag{6.5.5}$$

6.5 Magnetohydrodynamic Waves

$$-\mathrm{i}\omega\tilde{\rho}_{\mathrm{m}} + \mathrm{i}\rho_{\mathrm{m}0}\mathbf{k}\cdot\tilde{\mathbf{U}} = 0, \tag{6.5.6}$$

$$-\mathrm{i}\omega\rho_{\mathrm{m}0}\tilde{\mathbf{U}} = \frac{\mathrm{i}}{\mu_0}(\mathbf{k}\times\tilde{\mathbf{B}})\times\mathbf{B}_0 - \mathrm{i}\mathbf{k}\widetilde{P}, \tag{6.5.7}$$

$$-\mathrm{i}\omega\tilde{\mathbf{B}} = \mathrm{i}\mathbf{k}\times(\tilde{\mathbf{U}}\times\mathbf{B}_0), \tag{6.5.8}$$

$$\widetilde{P} = V_{\mathrm{S}}^2\,\tilde{\rho}_{\mathrm{m}}. \tag{6.5.9}$$

6.5 Magnetohydrodynamic Waves

$$\omega^2\tilde{\mathbf{U}} = \frac{1}{\mu_0\rho_{m0}}\{\mathbf{k}\times(\mathbf{k}\times[\tilde{\mathbf{U}}\times\mathbf{B}_0])\}\times\mathbf{B}_0 + V_S^2\mathbf{k}(\mathbf{k}\cdot\tilde{\mathbf{U}}). \qquad (6.5.12)$$

$$\left(\frac{\omega}{k}\right)^2\begin{bmatrix}\widetilde{U}_x\\ \widetilde{U}_y\\ \widetilde{U}_z\end{bmatrix} = V_A^2\begin{bmatrix}\widetilde{U}_x\\ \widetilde{U}_y\cos^2\theta\\ 0\end{bmatrix} + V_S^2\begin{bmatrix}\widetilde{U}_x\sin^2\theta+\widetilde{U}_z\sin\theta\cos\theta\\ 0\\ \widetilde{U}_x\sin\theta\cos\theta+\widetilde{U}_z\cos^2\theta\end{bmatrix}$$

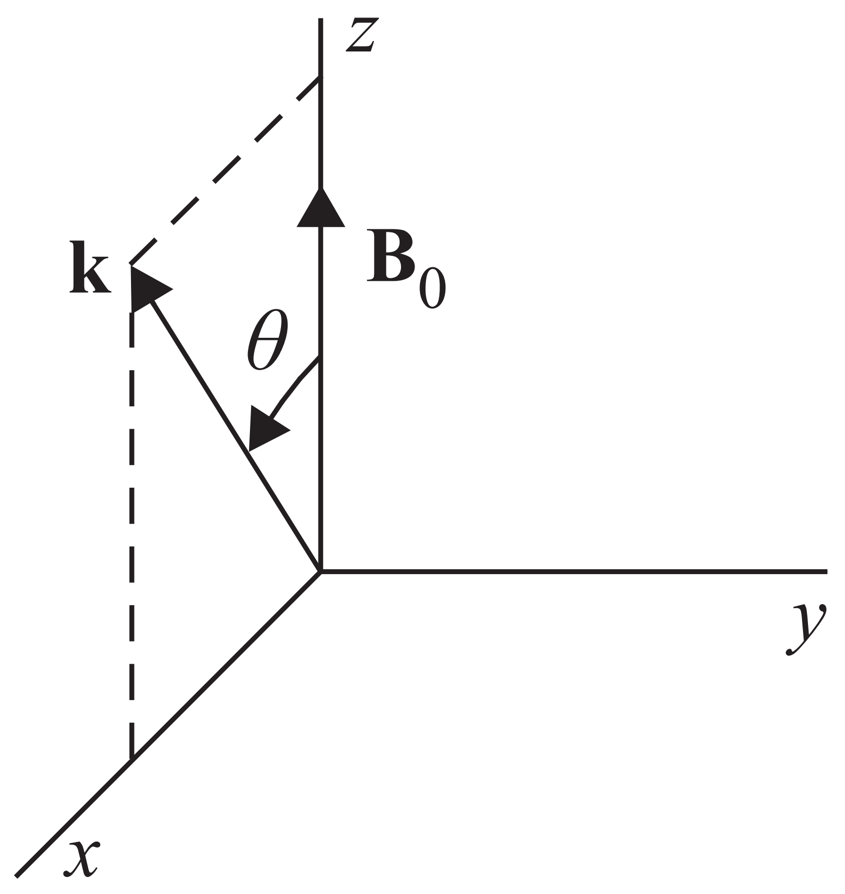

$$\cos\theta = k_{||}/k$$

$$\sin\theta = k_{\perp}/k$$

$$V_A = B_0/\sqrt{\mu_0\rho_{m0}}$$

6.5 Magnetohydrodynamic Waves

$$\begin{bmatrix} \upsilon_p^2 - V_S^2 \sin^2\theta - V_A^2 & 0 & -V_S^2 \sin\theta\cos\theta \\ 0 & \upsilon_p^2 - V_A^2\cos^2\theta & 0 \\ -V_S^2 \sin\theta\cos\theta & 0 & \upsilon_p^2 - V_S^2\cos^2\theta \end{bmatrix} \begin{bmatrix} \widetilde{U}_x \\ \widetilde{U}_y \\ \widetilde{U}_z \end{bmatrix} = 0. \quad (6.5.15)$$

$$\cos\theta = k_{||}/k$$

$$\sin\theta = k_{\perp}/k$$

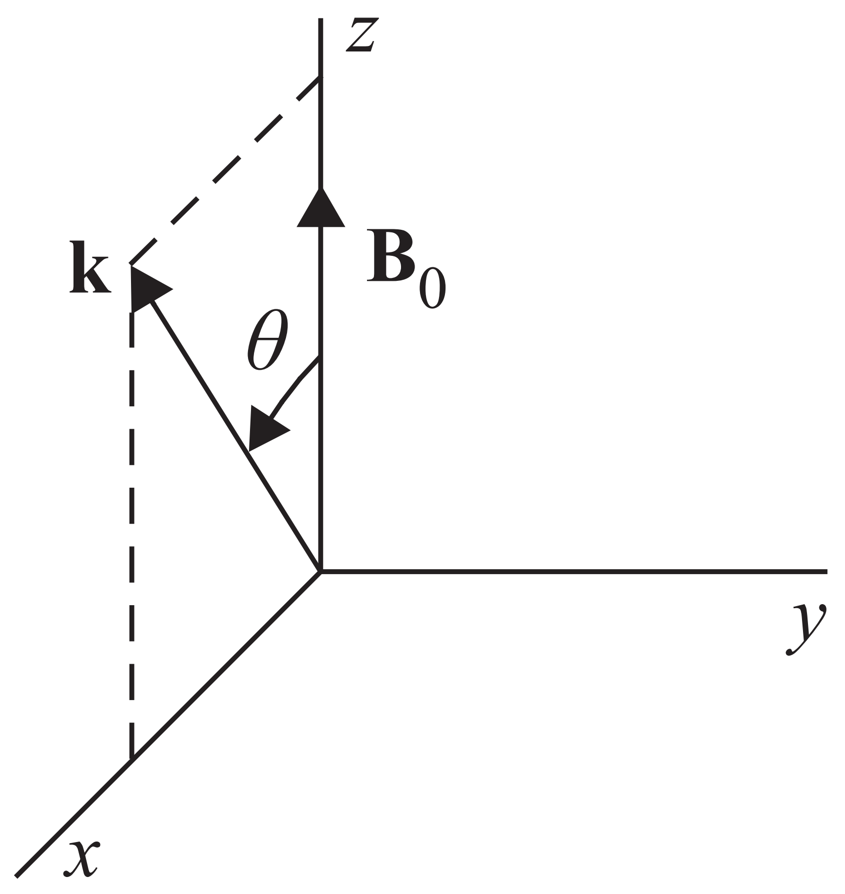

$$\upsilon_p = \omega/k$$

6.5 Magnetohydrodynamic Waves

This equation has non-trivial solutions for $\tilde{\mathbf{U}}$ if and only if the determinant of the matrix is zero, which gives the dispersion relation

$$Đ(k,\omega) = \left(\upsilon_{\mathrm{p}}^2 - V_{\mathrm{A}}^2 \cos^2\theta\right)\left[\upsilon_{\mathrm{p}}^4 - \upsilon_{\mathrm{p}}^2\left(V_{\mathrm{A}}^2 + V_{\mathrm{S}}^2\right) + V_{\mathrm{A}}^2 V_{\mathrm{S}}^2 \cos^2\theta\right] = 0. \tag{6.5.16}$$

It can be shown that the dispersion relation has three roots:

$$\upsilon_{\mathrm{p}}^2 = \frac{1}{2}\left(V_{\mathrm{A}}^2 + V_{\mathrm{S}}^2\right) - \frac{1}{2}\left[\left(V_{\mathrm{A}}^2 - V_{\mathrm{S}}^2\right)^2 + 4V_{\mathrm{A}}^2 V_{\mathrm{S}}^2 \sin^2\theta\right]^{1/2}, \tag{6.5.17}$$

$$\upsilon_{\mathrm{p}}^2 = V_{\mathrm{A}}^2 \cos^2\theta, \quad \leftarrow \text{Shear, or “transverse” Alfvén wave} \tag{6.5.18}$$

$$\upsilon_{\mathrm{p}}^2 = \frac{1}{2}\left(V_{\mathrm{A}}^2 + V_{\mathrm{S}}^2\right) + \frac{1}{2}\left[\left(V_{\mathrm{A}}^2 - V_{\mathrm{S}}^2\right)^2 + 4V_{\mathrm{A}}^2 V_{\mathrm{S}}^2 \sin^2\theta\right]^{1/2}. \tag{6.5.19}$$

6.5 Magnetohydrodynamic Waves

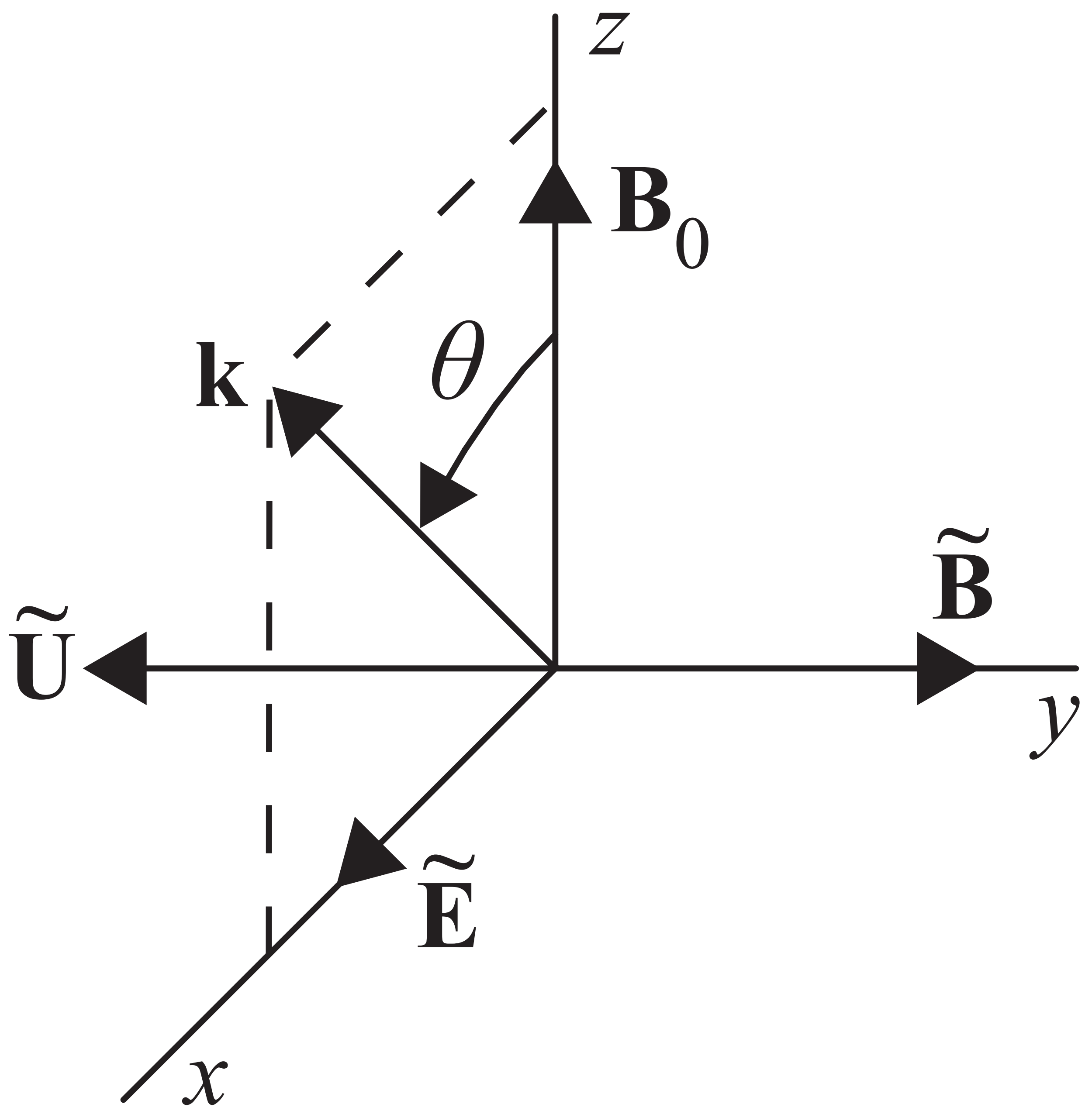

Shear Alfvén
Wave

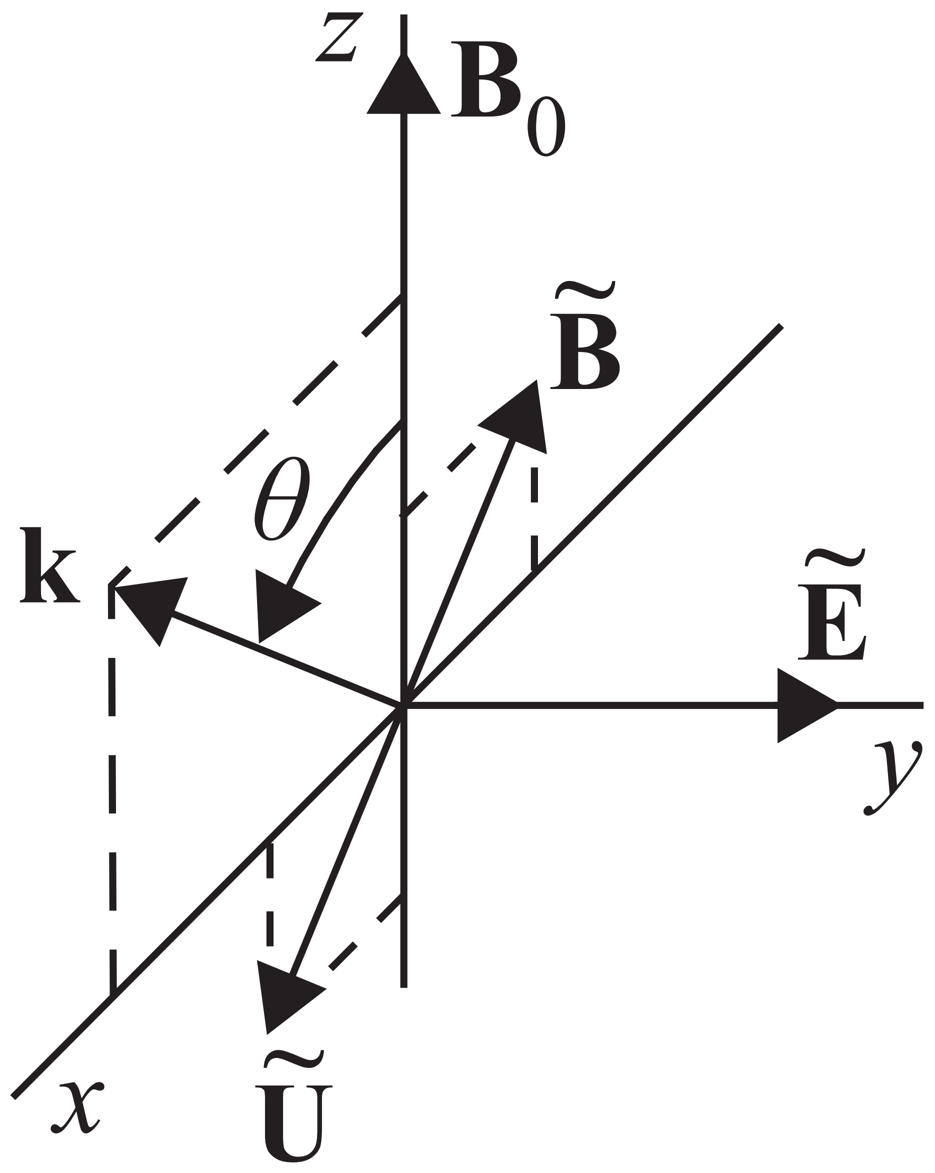

Fast magnetosonic
wave

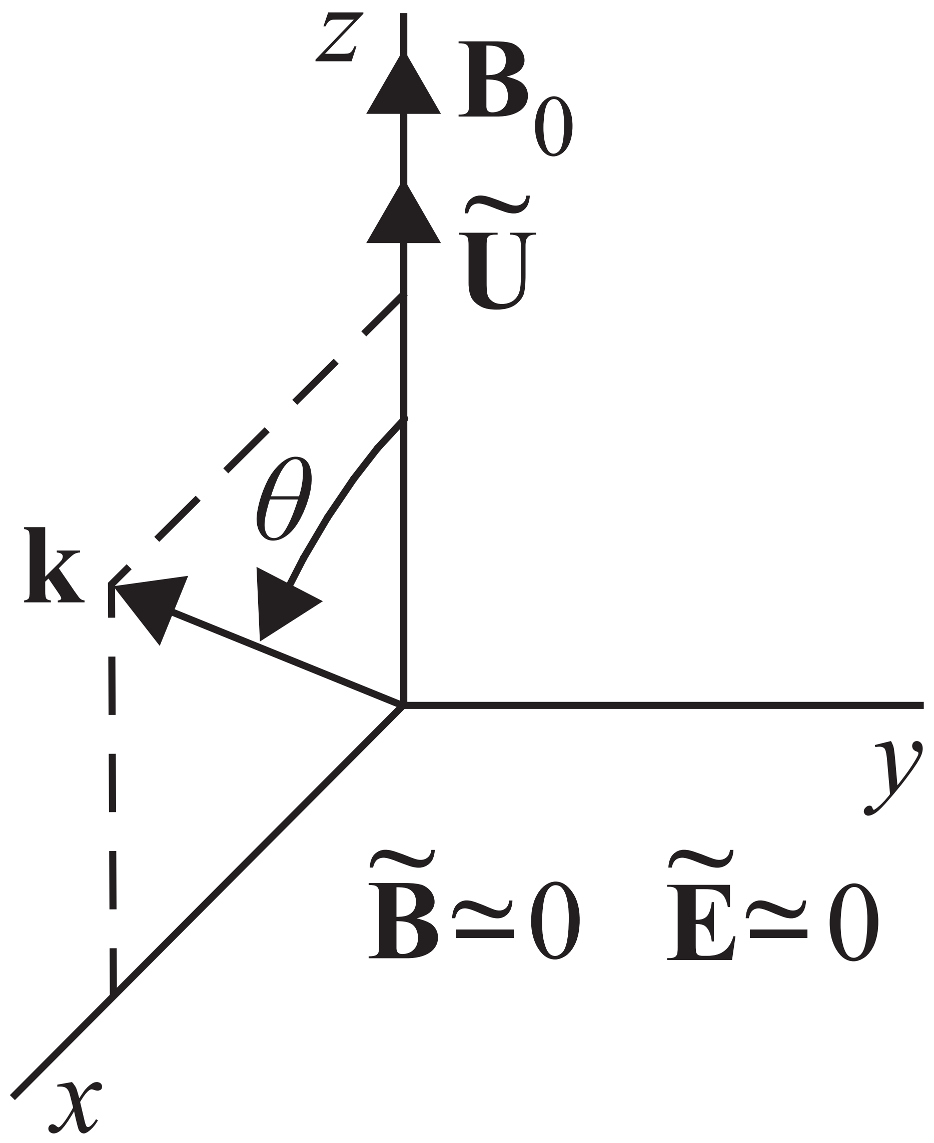

Slow magnetosonic
wave

6.5 Magnetohydrodynamic Waves

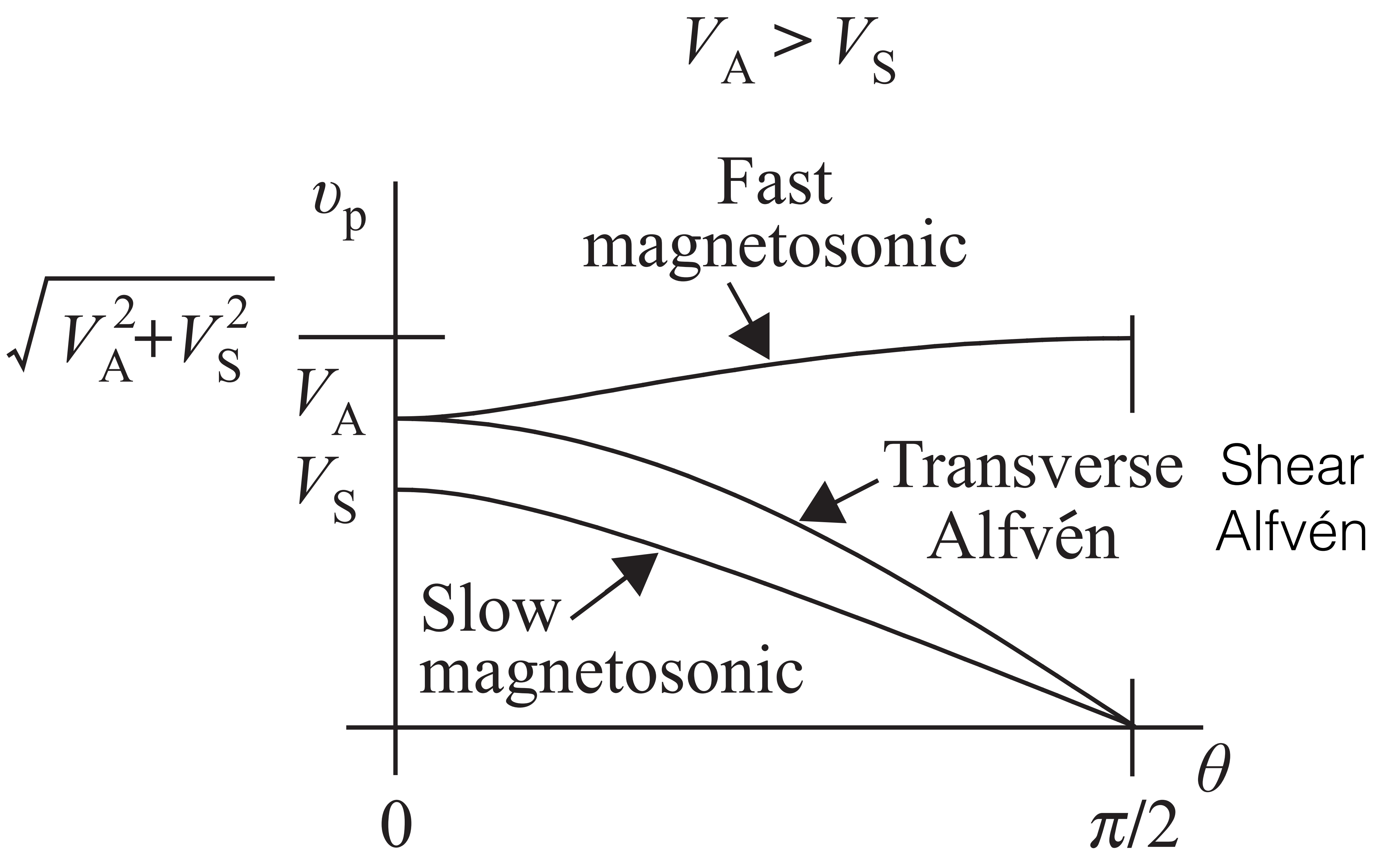

Figure 6.7 Plots of the phase velocities for the three MHD modes as a function of the wave normal angle for two cases, $V_A > V_S$ and $V_A < V_S$.

$$\beta \propto V_s^2/V_A^2$$

$$v_p = \omega/k$$

10.3 Electromagnetic Waves

$$\overleftrightarrow{\sigma} = \mathrm{i}\sum_s \frac{e_s^2 n_s}{m_s\omega_{\mathrm{c}s}} \sum_n \int_{-\infty}^{\infty}\int_0^{\infty} \frac{2\pi\upsilon_\perp \mathrm{d}\upsilon_\perp \mathrm{d}\upsilon_\parallel}{\alpha_s + n} \times \begin{bmatrix} A_s \dfrac{n^2\upsilon_\perp}{\beta_s^2} J_n^2 & \mathrm{i}A_s \dfrac{n\upsilon_\perp}{\beta_s} J_n J_n' & B_s \dfrac{n\upsilon_\perp}{\beta_s} J_n^2 \\ -\mathrm{i}A_s \dfrac{n\upsilon_\perp}{\beta_s} J_n J_n' & A_s \upsilon_\perp J_n' J_n' & -\mathrm{i}B_s \upsilon_\perp J_n J_n' \\ A_s \dfrac{n\upsilon_\parallel}{\beta_s} J_n^2 & \mathrm{i}A_s \upsilon_\parallel J_n J_n' & B_s \upsilon_\parallel J_n^2 \end{bmatrix}, \qquad (10.3.18)$$

$$\begin{bmatrix} K_{xx} - \dfrac{c^2k^2}{\omega^2}\cos^2\theta & K_{xy} & K_{xz} + \dfrac{c^2k^2}{\omega^2}\sin\theta\cos\theta \\ K_{yx} & K_{yy} - \dfrac{c^2k^2}{\omega^2} & K_{yz} \\ K_{zx} + \dfrac{c^2k^2}{\omega^2}\sin\theta\cos\theta & K_{zy} & K_{zz} - \dfrac{c^2k^2}{\omega^2}\sin\theta \end{bmatrix} \begin{bmatrix} \widetilde{E}_x \\ \widetilde{E}_y \\ \widetilde{E}_z \end{bmatrix} = 0. \quad (10.3.28)$$

JOURNAL OF GEOPHYSICAL RESEARCH, VOL. 101, NO. A3, PAGES 5085–5094, MARCH 1, 1996

On the kinetic dispersion relation for shear Alfvén waves

Robert L. Lysak

School of Physics and Astronomy, University of Minnesota, Minneapolis

William Lotko

Thayer School of Engineering, Dartmouth College, Hanover, New Hampsh

$$\left(\frac{\omega}{k_{\parallel} V_A}\right)^2 \approx 1 + k_{\perp}^2\left(\rho_s^2 + \frac{3}{4}\rho_i^2\right)$$

is predominantly parallel. Then the dispersion relation for the kinetic Alfvén wave is given by the determinant of the 2×2 matrix

$$\det\begin{pmatrix} \frac{c^2}{V_A^2}\frac{1-\Gamma_0(\mu_i)}{\mu_i} - n_{\parallel}^2 & n_{\parallel}n_{\perp} \\ n_{\parallel}n_{\perp} & \frac{\Gamma_0(\mu_e)}{k_{\parallel}^2\lambda_{De}^2}\left(1+\xi Z(\xi)\right) - n_{\perp}^2 \end{pmatrix} = 0 \quad (5)$$

In this dispersion relation, it has been assumed that $c^2 / V_A^2 \gg 1$ and that $k_{\parallel}^2\lambda_{De}^2 \ll 1$, so that the unit terms in the diagonal elements can be dropped. Here $n_{\parallel} = k_{\parallel}c/\omega$, $n_{\perp} = k_{\perp}c/\omega$, $\mu_i = k_{\perp}^2\rho_i^2$, $\mu_e = k_{\perp}^2\rho_e^2$, $\xi = \omega / k_{\parallel}a_e$, $a_e = (2T_e/m_e)^{1/2}$, Γ_0 is the modified Bessel function $\Gamma_0(\mu) = e^{-\mu}I_0(\mu)$, and Z is the usual plasma dispersion function [*Fried and Conte*, 1961]. Definitions of other symbols in

Alfvén Waves in Tokamaks

- Antenna excitation of kinetic Alfvén wave (KAW) and the Alfvén wave resonance
  - "The Alfvén wave spectrum as measured on a tokamak," Collins, et al., *Physics of Fluids* 29, 2260 (1986); https://doi.org/10.1063/1.865563
  - "Mode Conversion to the Kinetic Alfven Wave in Low-Frequency Heating Experiments in the TCA Tokamak," H. Weisen, et al., *Phys Rev Letters*, 63, 22 (1989)
- Energetic particle excitation of toroidal Alfvén eigenmodes
  - "Basic physics of Alfvén instabilities driven by energetic particles in toroidally confined plasmas," Bill Heidbrink, *Phys Plasmas*, 15, 055501 (2008)

TCA

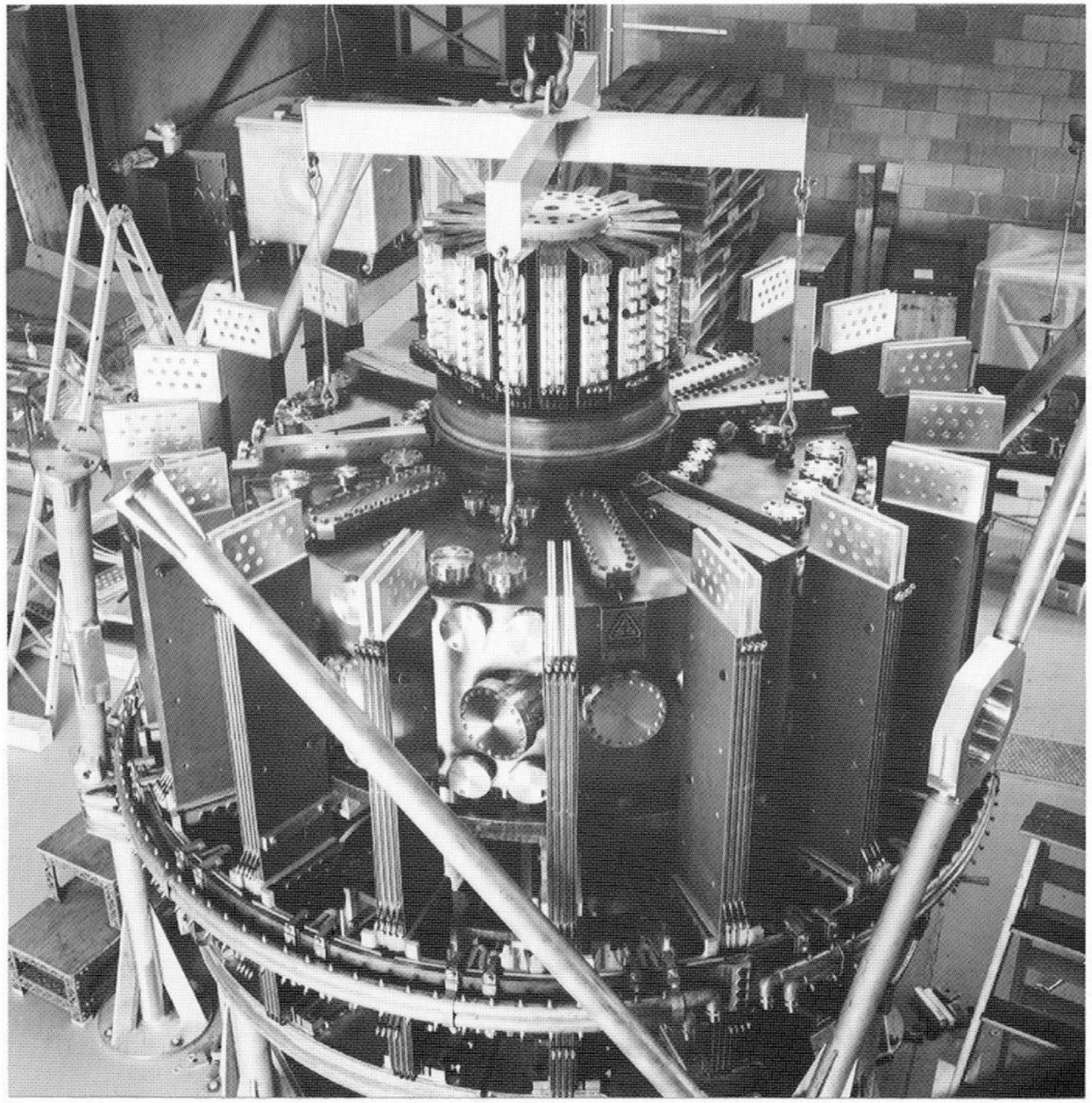

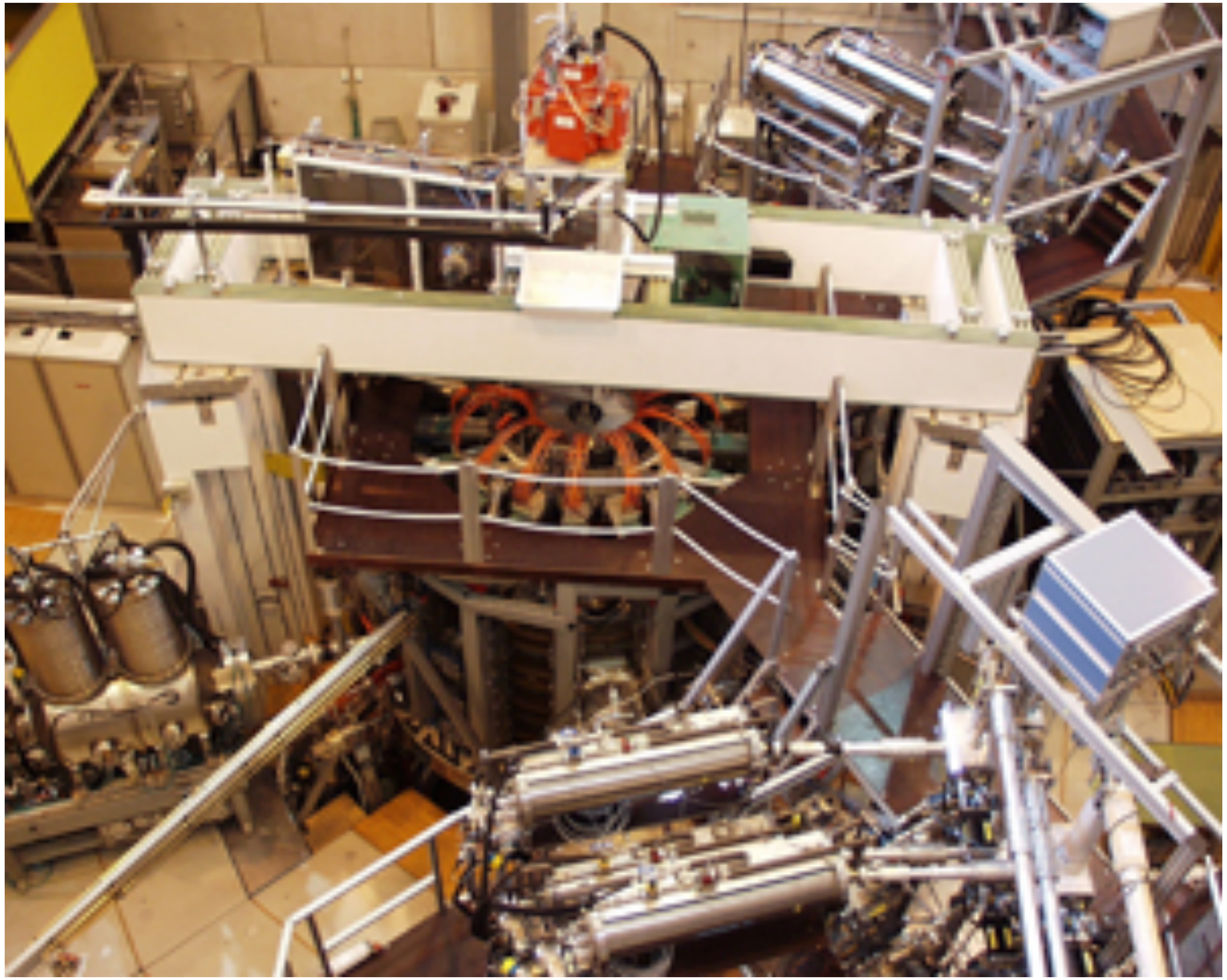

TCA

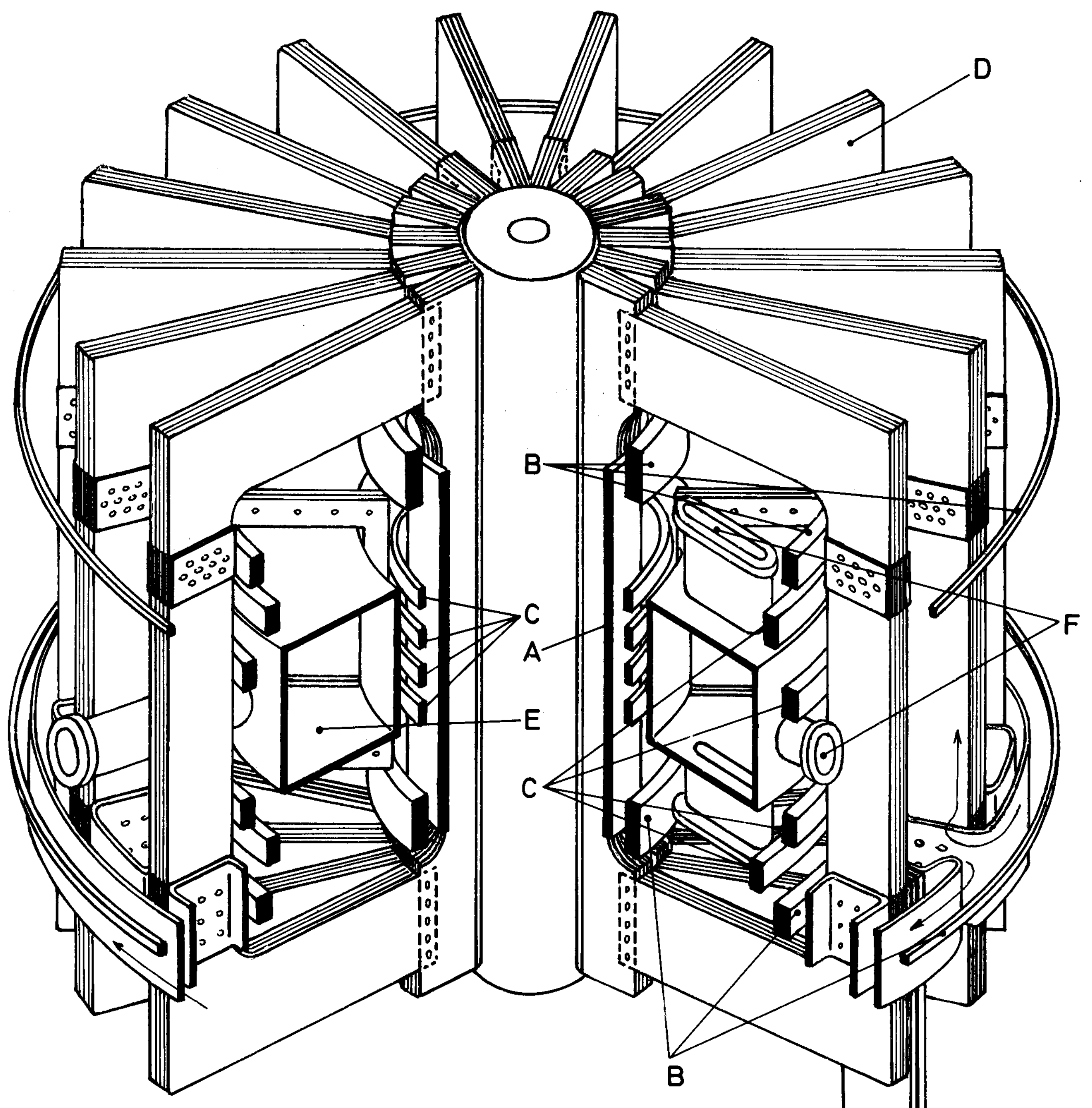

A bobine pour chauffage ohmique
B bobines auxiliaires (6) pour minimiser le champ de fuite de la bobine A
C bobines du champ vertical (8)
D bobine de champ toroïdal
E chambre à vide toroïdale
F accès pour les diagnostics

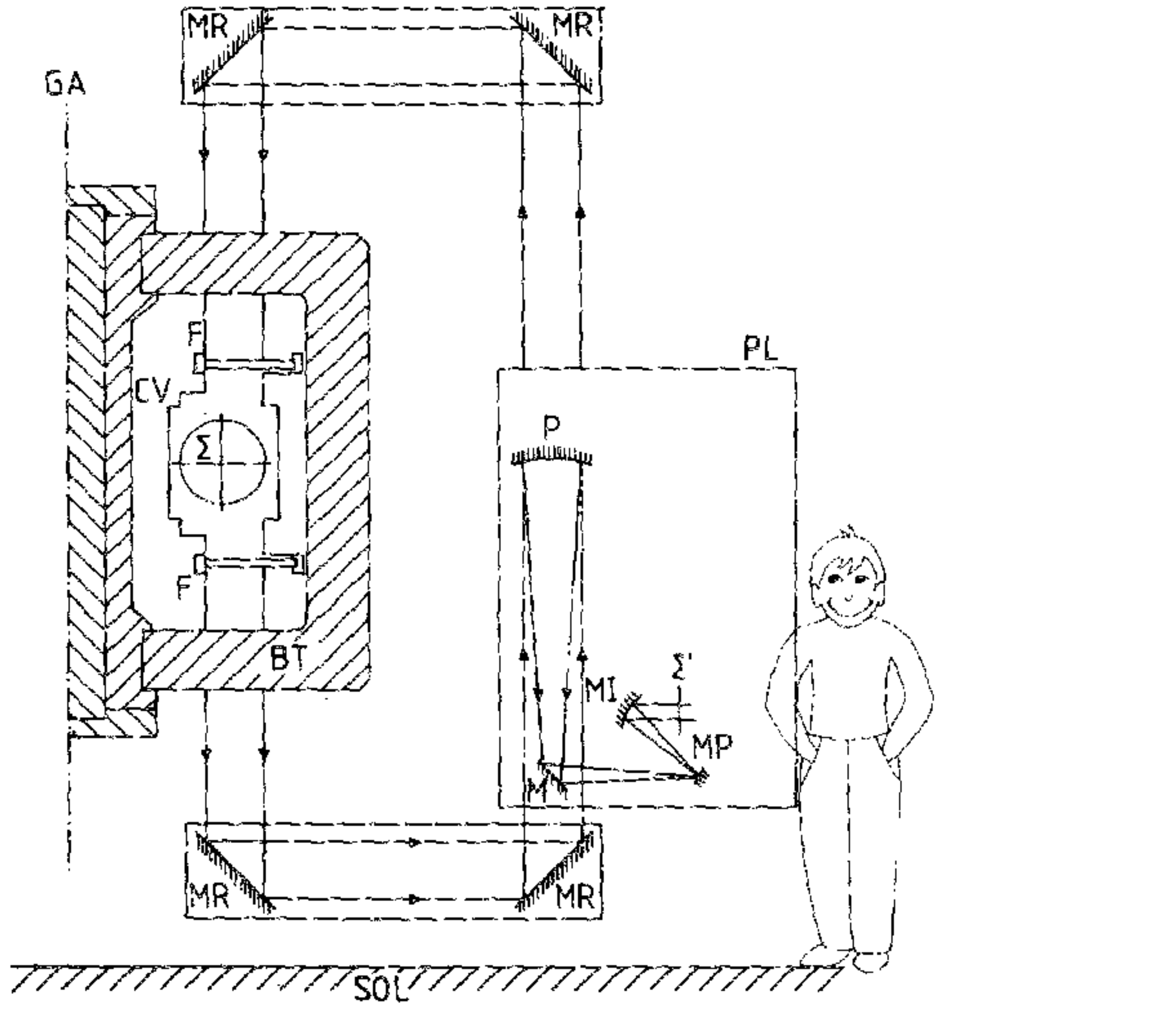

FIG. 3. Optical arrangement on the TCA tokamak. PL: optical table; P: parabolic mirror ($f = 190.5$ cm); M: flat mirror; MP: phase mirror; MR: relay mirror; F: NaCl vacuum window; CV: vacuum chamber; BT: toroidal field coil; GA: major axis; Σ: object plane at plasma midplane; Σ': image plane (imaging optics simplified).

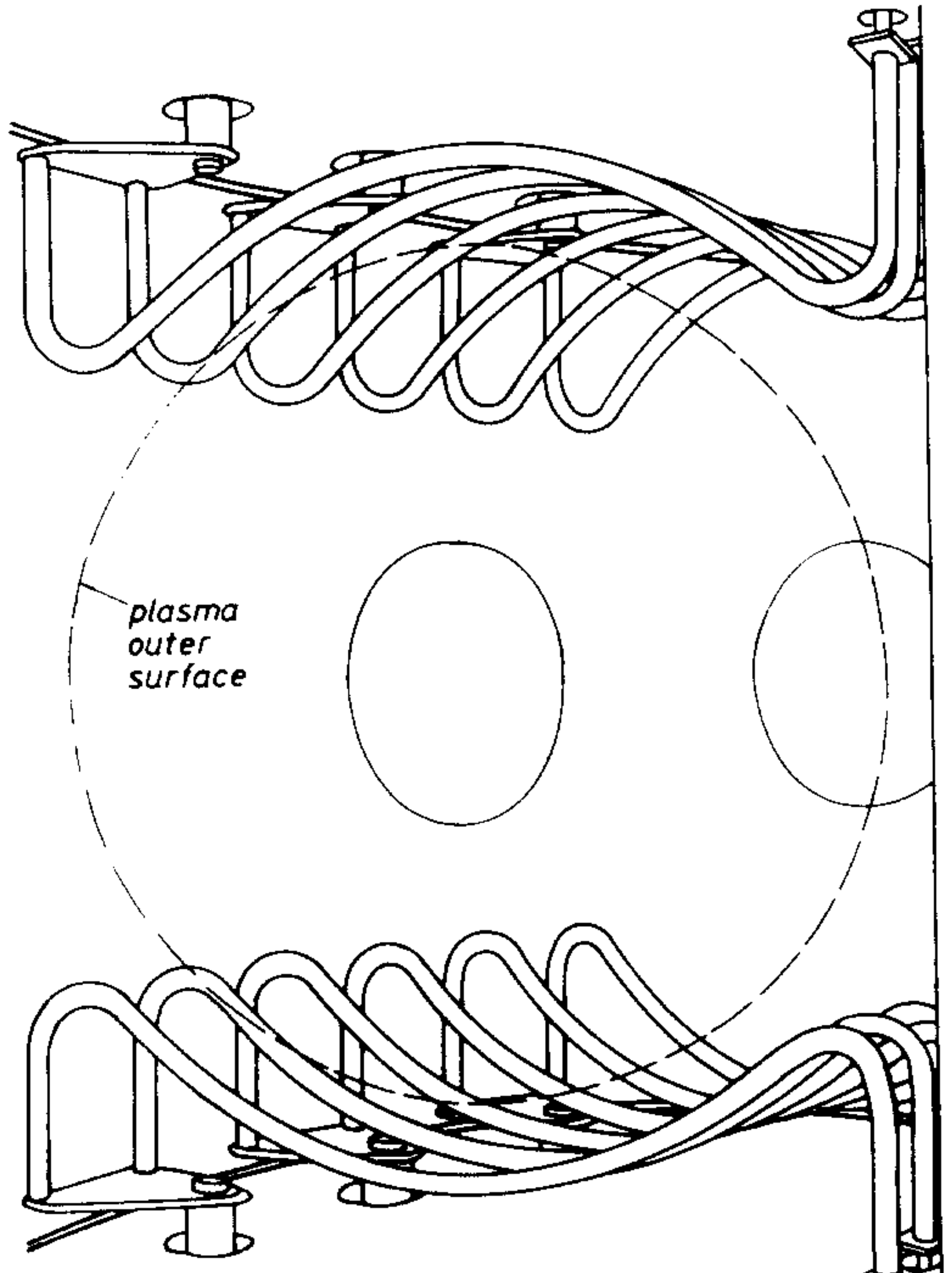

FIG. 1. Design of the TCA antennas: (a) vertical section, (b) horizontal section, and (c) perspective.

Measurement of KAW Excitation

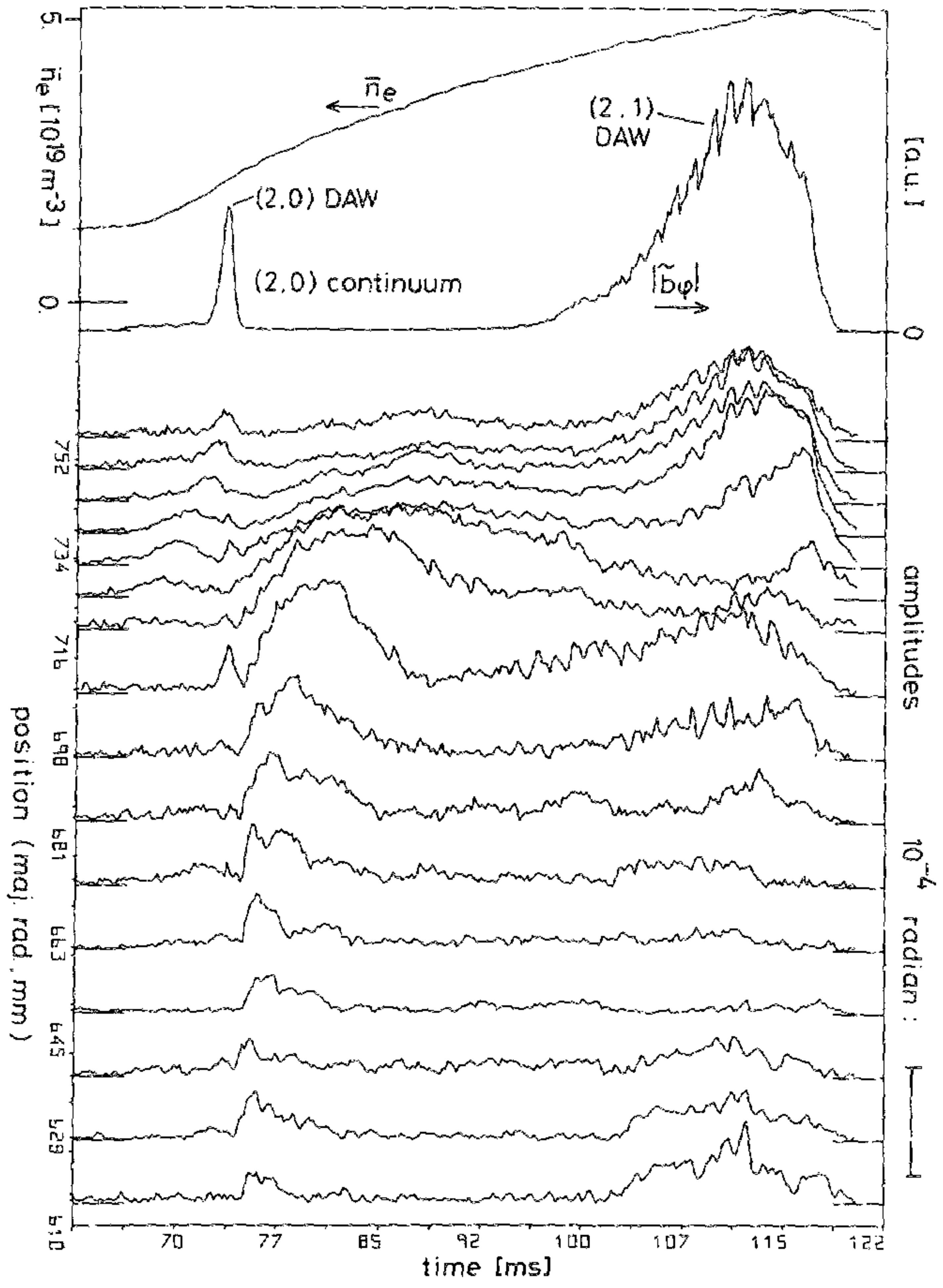

FIG. 9. Example of evolution of the synchronous density oscillation amplitude profile in an Alfvén wave heating discharge.

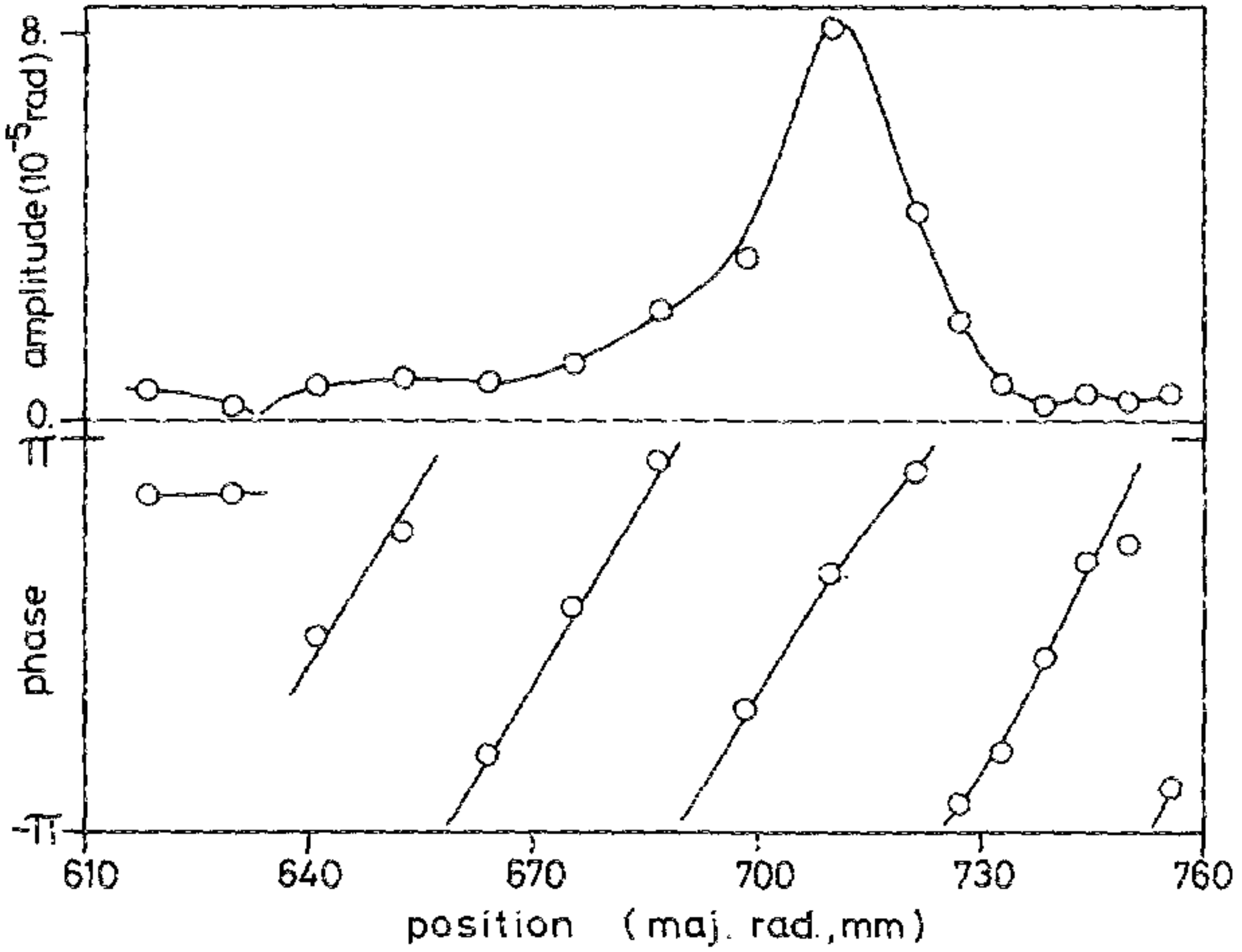

FIG. 10. Profile of amplitude and phase of synchronous density oscillations due to the kinetic Alfvén wave [(2, 0) continuum].

Observations of Toroidal Coupling for Low-n Alfvén Modes in the TCA Tokamak

K. Appert, G. A. Collins, F. Hofmann, R. Keller, A. Lietti, J. B. Lister, A. Pochelon, and L. Villard
Centre de Recherches en Physique des Plasmas, Association Euratom–Confédération Suisse, Ecole Polytechnique Fédérale de Lausanne, CH-1007 Lausanne, Switzerland
(Received 21 November 1984)

The antenna structure in the TCA tokamak is phased to excite preferentially Alfvén waves with known toroidal and poloidal wave numbers. Surprisingly, the loading spectrum includes both discrete and continuum modes with poloidal wave numbers incompatible with the antenna phasing. These additional modes, which are important for our heating experiments, can be attributed to linear mode coupling induced by the toroidicity of the plasma column, when we take into account ion-cyclotron effects.

The antenna is designed to excite a compressional or fast magnetosonic wave which converts to the kinetic Alfvén wave at a radius r_0 defined by the Alfvén resonance condition, given in the large–aspect-ratio approximation by

$$\frac{n+m/q(r_0)}{R}=k_A(r_0)\equiv\frac{\omega(1-\omega^2/\omega_{ci}^2)^{-1/2}}{V_A(r_0)}, \quad (1)$$

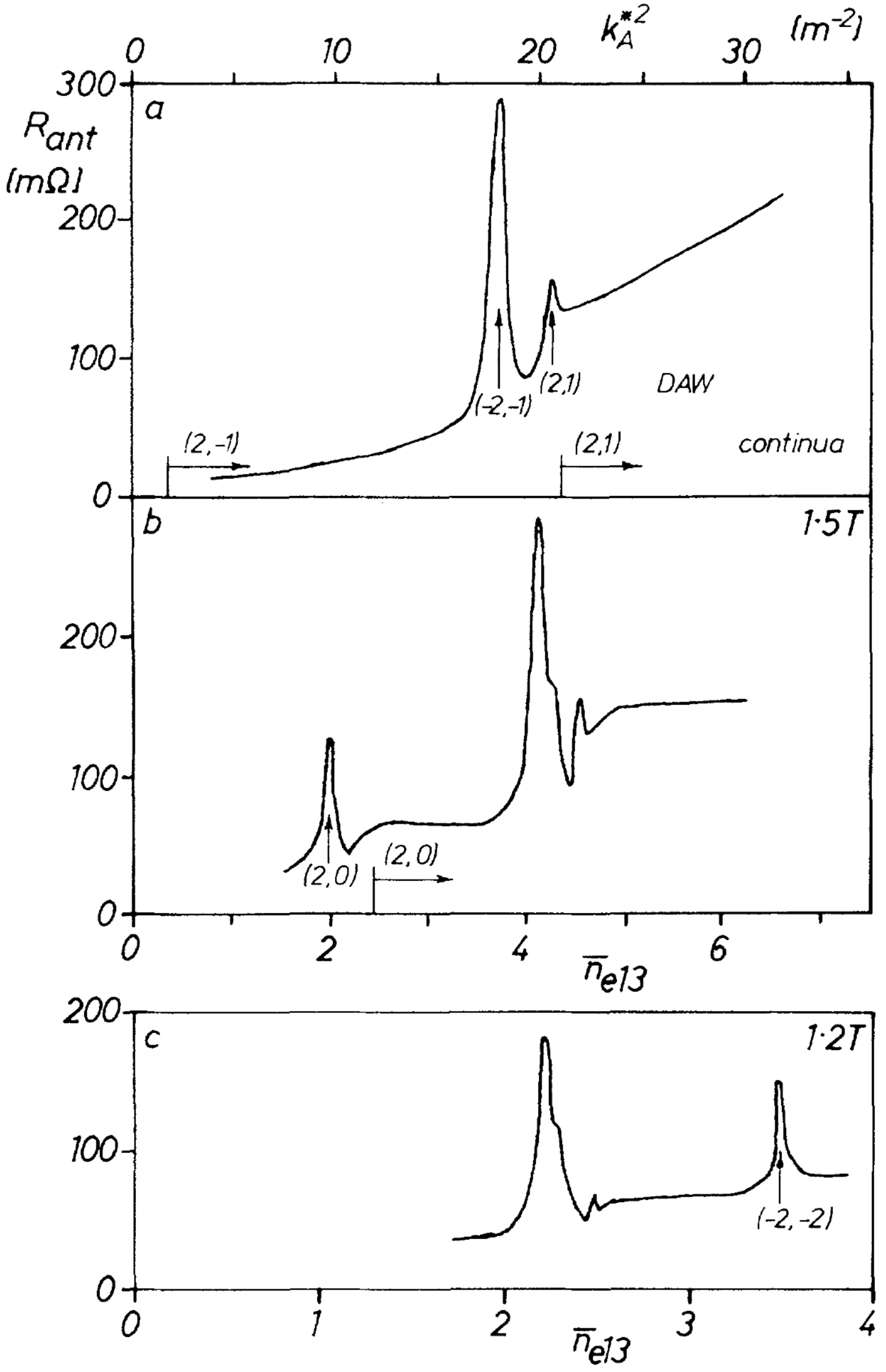

FIG. 1. Loading per antenna group as a function of line-averaged electron density ($N=2$, $M=1$, deuterium plasma). (a) Cylindrical calculation; (b) measurements in standard conditions; (c) measurements at lower toroidal field and with side shields.

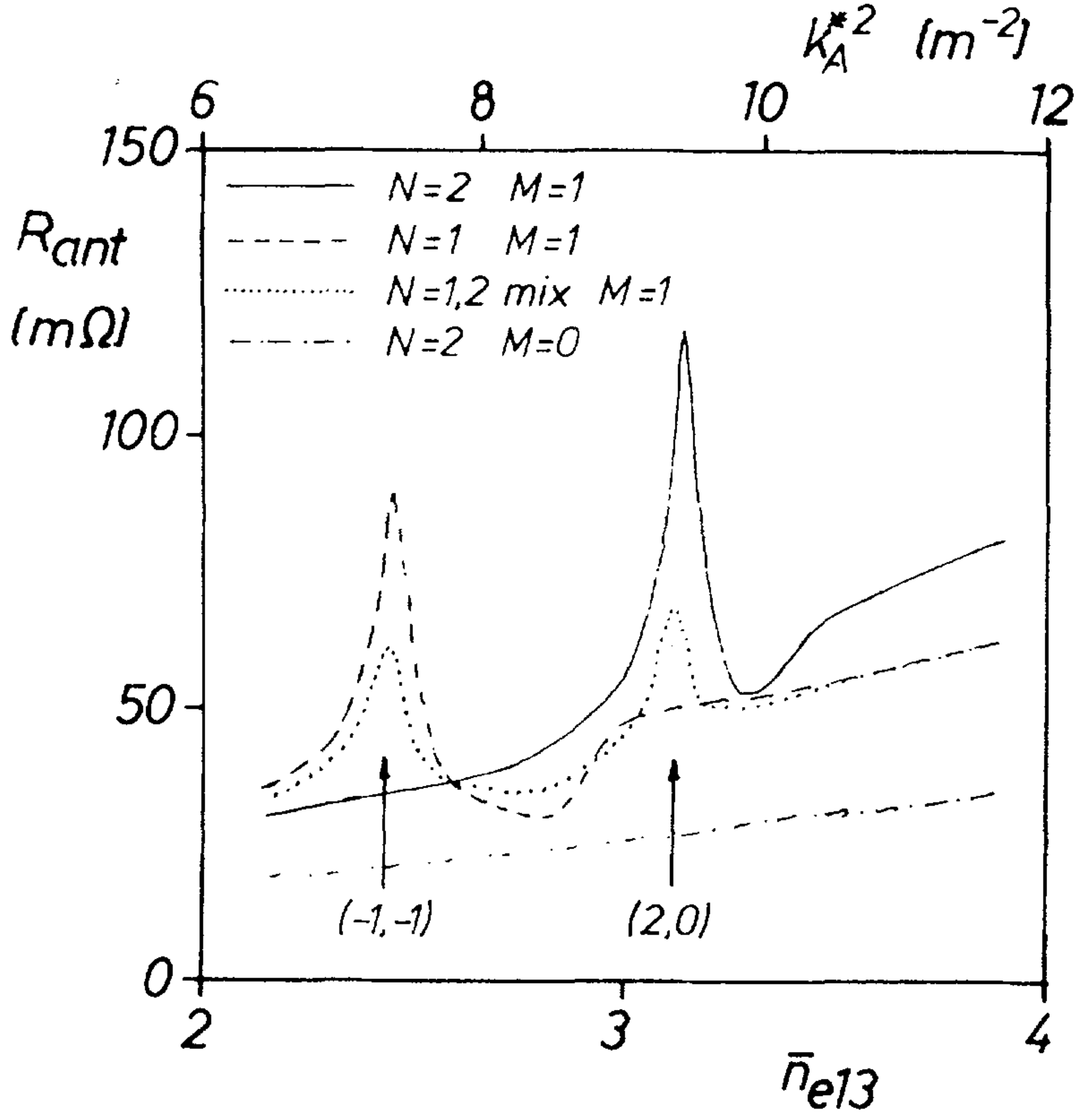

FIG. 2. Loading near the (2,0) threshold measured for different antenna phasings (hydrogen plasma).

Mode Conversion to the Kinetic Alfvén Wave in Low-Frequency Heating Experiments in the TCA Tokamak

H. Weisen, K. Appert, G. G. Borg, B. Joye, A. J. Knight, J. B. Lister, and J. Vaclavik
Centre de Recherches en Physique des Plasmas, Association Euratom–Confédération Suisse, Ecole Polytechnique Fédérale de Lausanne, 21, Avenue des Bains, CH-1007 Lausanne, Switzerland
(Received 11 April 1989)

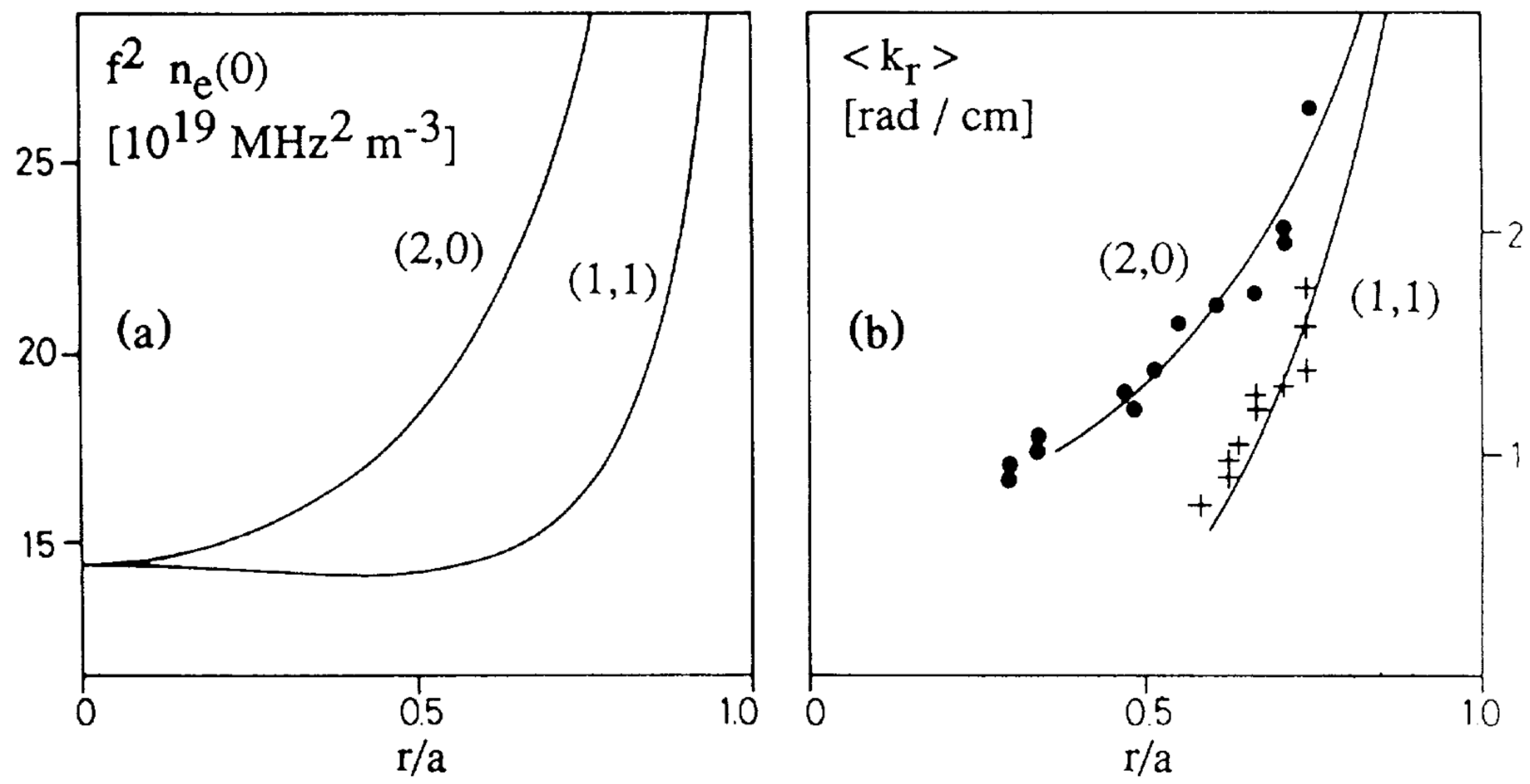

FIG. 1. (a) Resonance position as a function of frequency and central density for modeled mass density and current profiles. (b) Mean radial wave number as a function of position (averaged over one cycle of propagation). The solid lines are obtained from the KAW dispersion relation.

function of the position of the amplitude maximum. The solid lines were obtained from the approximate dispersion relation for the KAW expressed as

$$k_r^2\rho_i^2(\tfrac{3}{4}+T_e/T_i)=(\omega^2-k_\parallel^2V_A^2)/k_\parallel^2V_A^2\,, \tag{2}$$

where ρ_i is the ion Larmor radius. Although this relation is only valid for a homogeneous plasma, the k_r obtained by replacing V_A^2 by a linearly position-dependent V_A^2 about the resonance layer agrees well with the wavelength predicted by Hasegawa and Chen's original calculation[3] for a linear density profile. In this simple com-

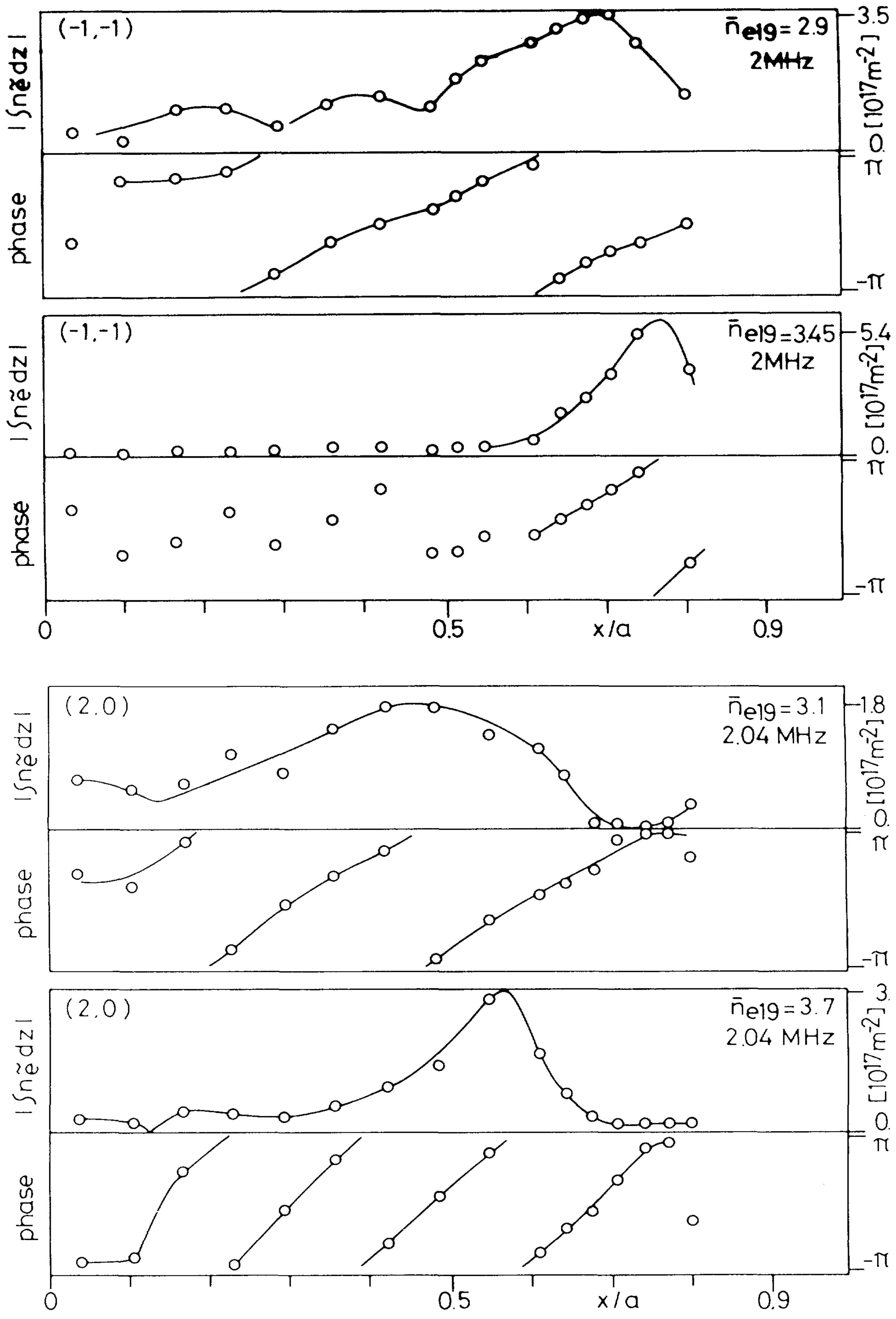

FIG. 2. Examples of observed profiles of line density fluctuations in the $(-1,-1)$ and (2,0) continua.

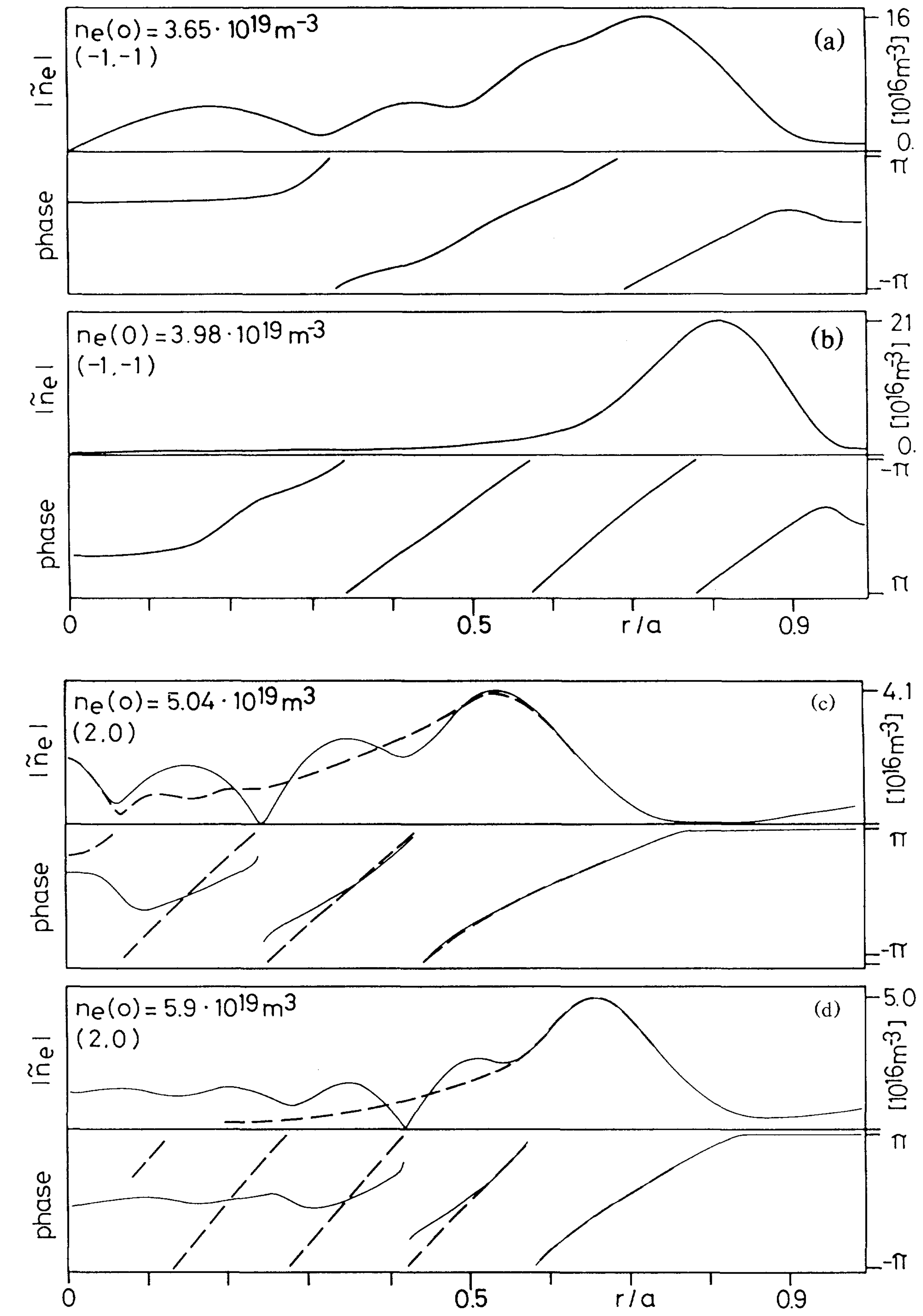

FIG. 3. Examples of calculated density fluctuations in the $(-1,-1)$ and (2,0) continua. The resonance layer positions were chosen to match those of Fig. 2. The broken lines of (c) and (d) for the (2,0) KAW represent the remaining wave field after subtraction of the fast-wave mode.

$$k_r^2 \rho_i^2 (\tfrac{3}{4} + T_e/T_i) = (\omega^2 - k_\parallel^2 V_A^2)/k_\parallel^2 V_A^2 , \qquad (2)$$

Measurements of the Tokamak-Safety-Factor Profile by Means of Driven Resonant Alfvén Waves

H. Weisen, G. Borg, B. Joye, A. J. Knight, and J. B. Lister

Centre de Recherches en Physique des Plasmas, Association EURATOM–Confédération Suisse, Ecole Polytechnique Fédérale de Lausanne, 21, av. des Bains, CH-1007 Lausanne, Switzerland

(Received 25 July 1988)

We report on the first measurements of the tokamak-safety-factor profile by means of Alfvén waves. The waves were launched by use of the TCA tokamak Alfvén-wave heating antennae. The associated density oscillation profiles provided the Alfvén-wave resonance layer positions which depend on the local value of the safety factor, q. Our results show a time-averaged q profile with a flat central region with q close to unity.

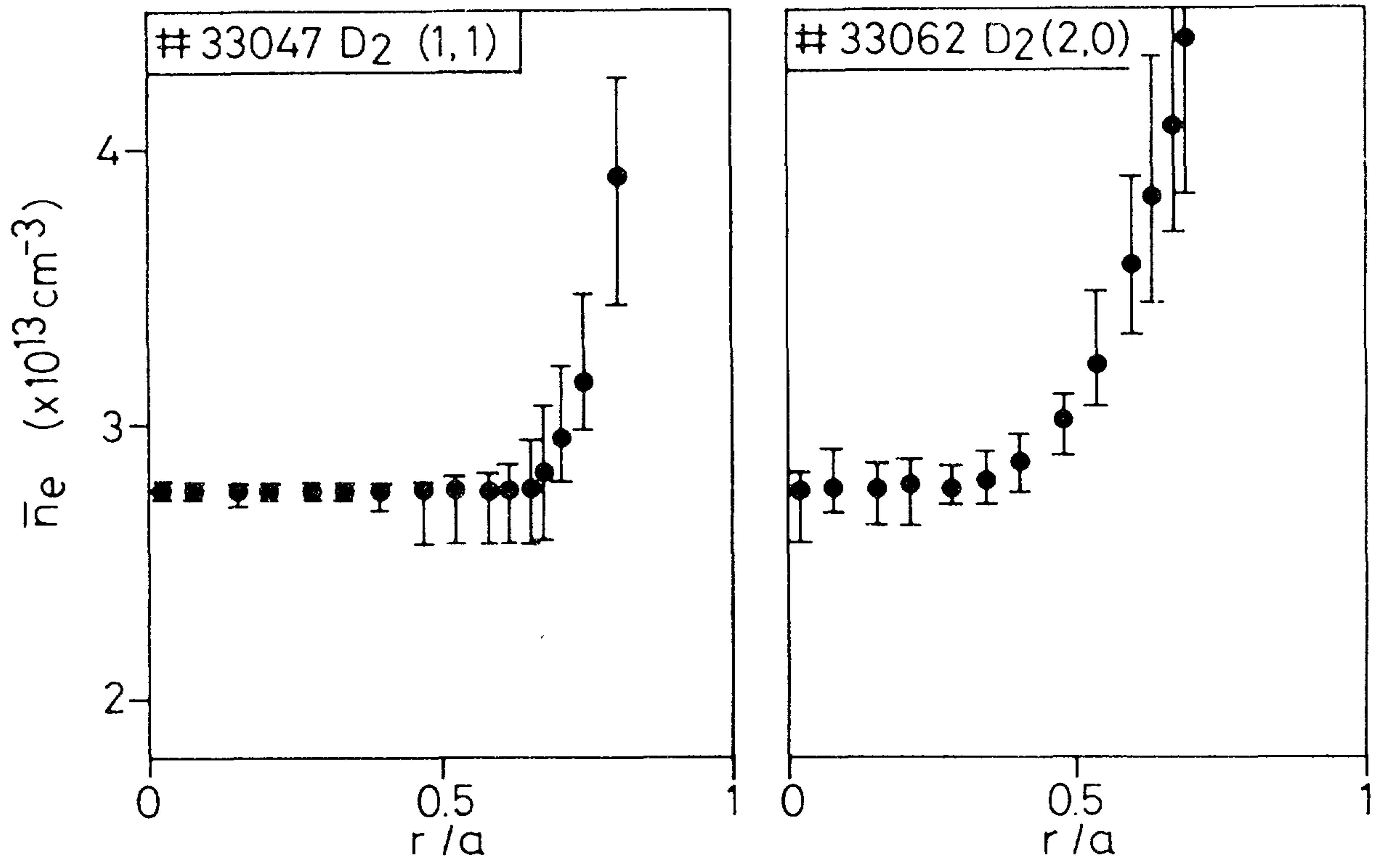

FIG. 4. Resonance layer positions for the (1,1) and (2,0) modes as a function of the central line density.

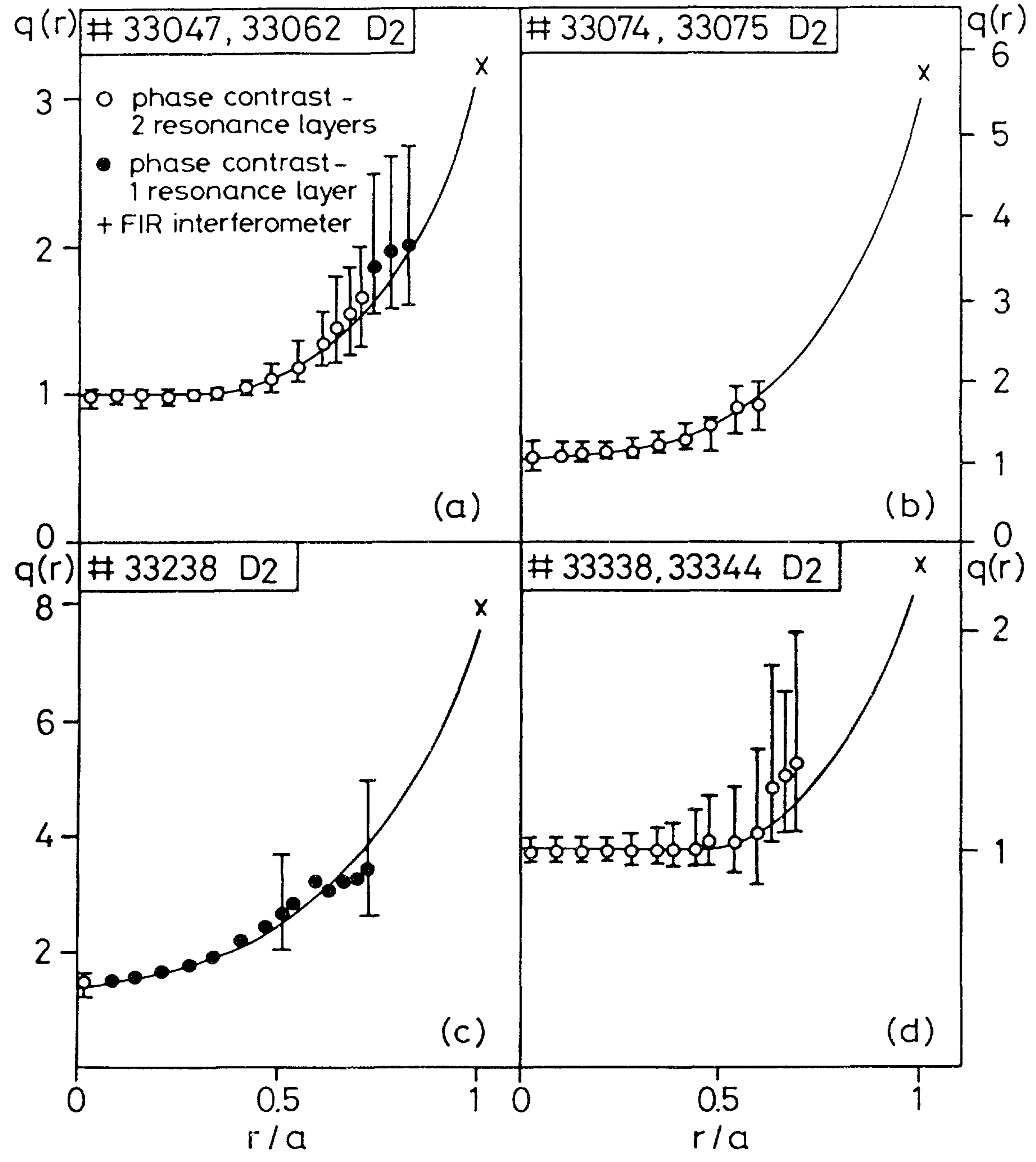

FIG. 5. Safety-factor profiles for (a) $B_\phi = 1.51$ T, $I_p = 125$ kA, (b) $B_\phi = 1.51$ T, $I_p = 70$ kA, (c) $B_\phi = 1.51$ T, $I_p = 50$ kA, (d) $B_\phi = 1.16$ T, $I_p = 135$ kA.

JOURNAL OF APPLIED PHYSICS VOLUME 30, NUMBER 11 NOVEMBER, 1959

Look!

Space Charge Waves in Cylindrical Plasma Columns*

A. W. TRIVELPIECE† AND R. W. GOULD
California Institute of Technology, Pasadena, California

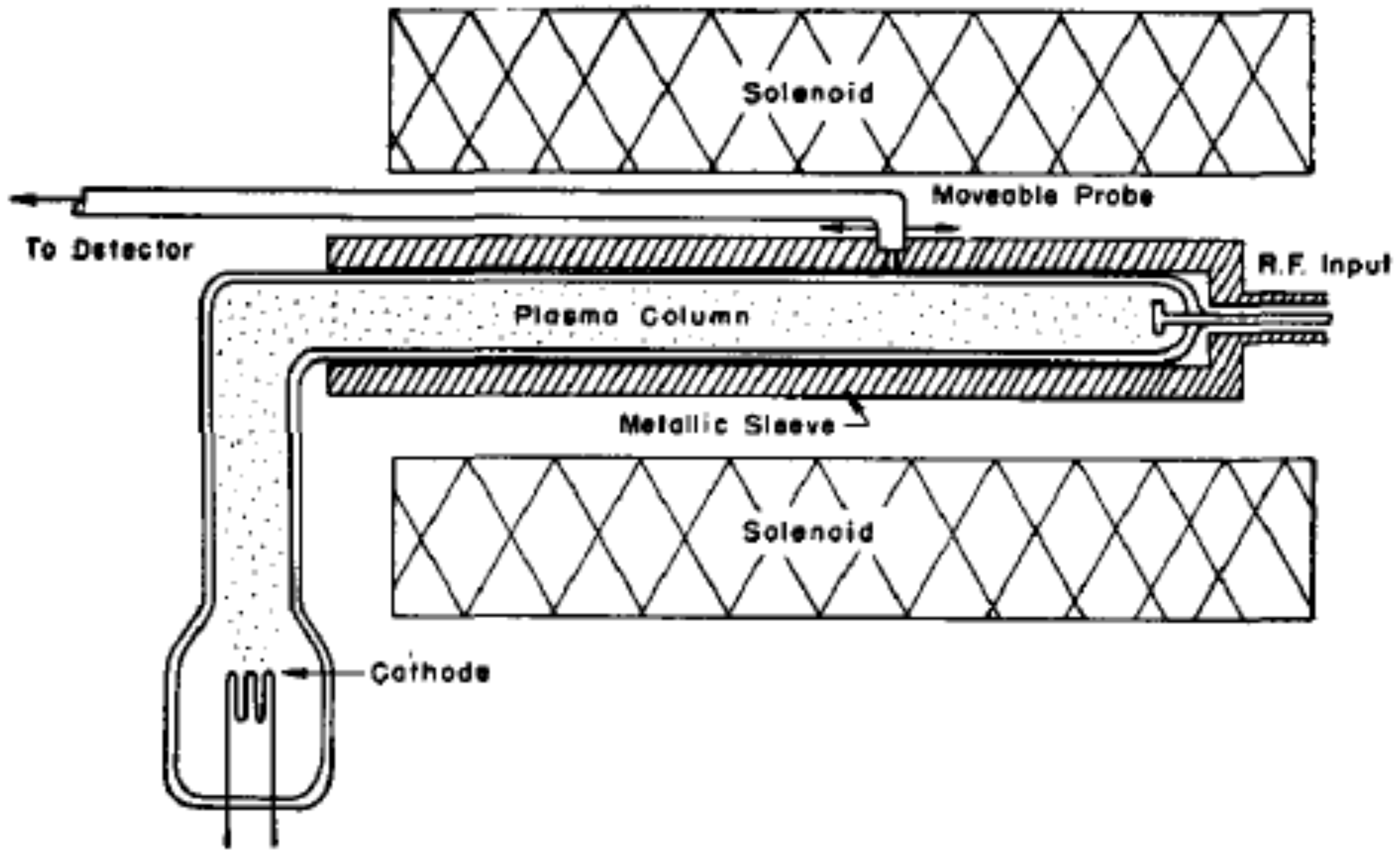

FIG. 10. Schematic of apparatus to measure phase and attenuation characteristics of space charge waves in a plasma.

TABLE I. Pertinent dimensions of experimental apparatus used in space charge wave propagation experiment.

Diameter of plasma	0.328 in.
Diameter of tube containing plasma	0.410 in.
Diameter of slotted wave guide	0.410 and 0.750 in.
Length of plasma column	25 cm
Signal frequency range	10 to 4000 mc
Cyclotron frequency range	0 to 5000 mc
Plasma frequency range	500 to 5000 mc
Temperature of mercury in tube	300±0.1°K
Empty wave guide cutoff frequency (approx)	25 000 mc
Pressure of mercury at 300°K (approx)	2 microns
Mean free path of plasma electrons (approx)	5 cm

Assuming wave solutions $\exp[j(\omega t-\beta z)]$

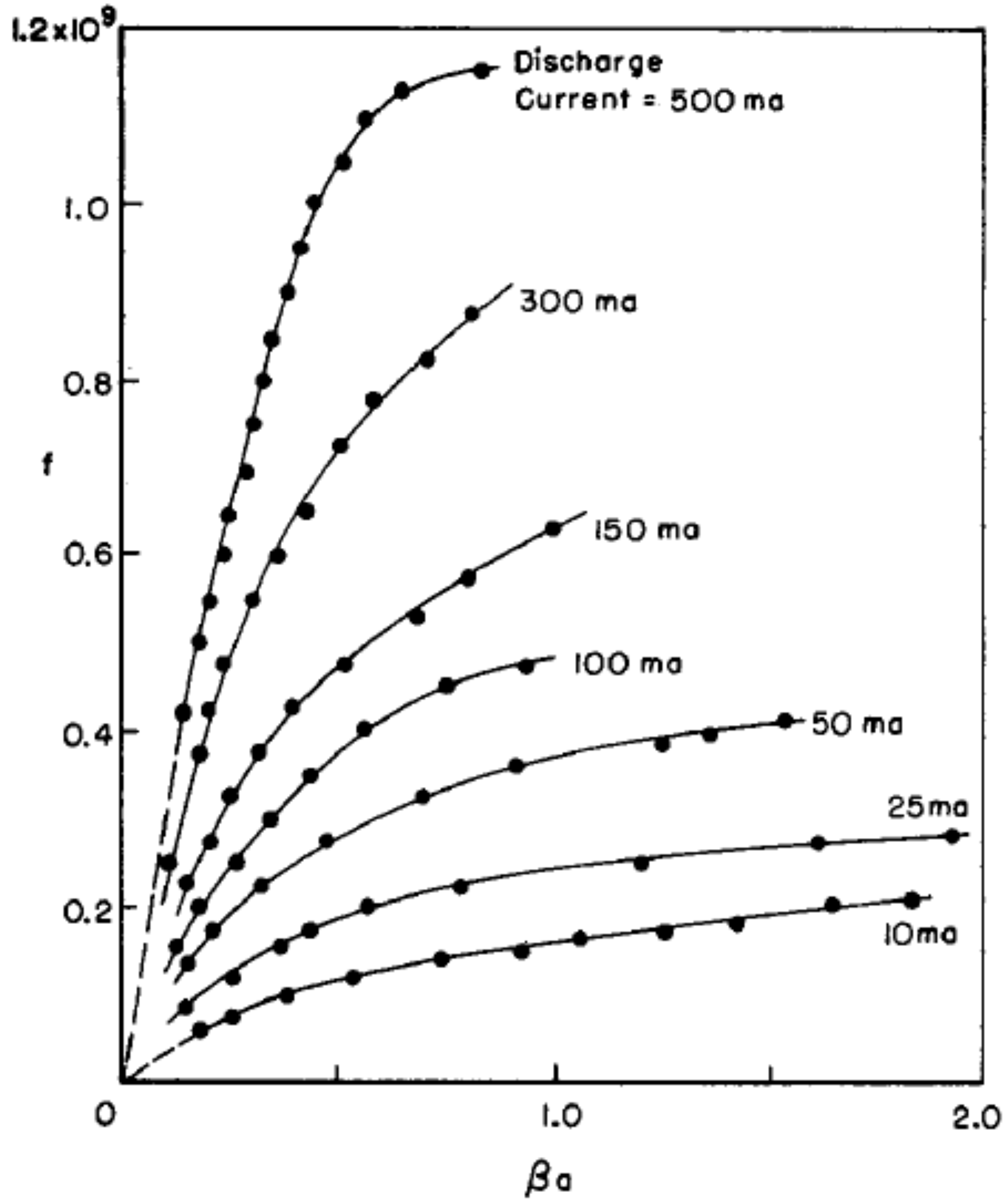

FIG. 13. Measured phase characteristics of plasma space charge waves for no magnetic field for $a=0.52$ cm, $b=0.62$ cm, $K=4.6$.

TG Modes: Low Frequency Surface Waves

INSIDE PLASMA ($r < a$): $\bar{E} = -\nabla \Phi$ $\quad \nabla \cdot (\epsilon_0 K \bar{E}) = 0$ $\quad K = 1 - \frac{\omega_p^2}{\omega^2}$

$$\Rightarrow \nabla^2 \Phi = 0$$

OUTSIDE PLASMA ($r > a$): $\bar{E} = -\nabla \Phi$ $\quad \nabla \cdot (\epsilon_0 \bar{E}) = 0$

$$\nabla^2 \Phi = 0$$

BOUNDARY CONDITIONS ($r = a$):

$$\hat{n} \cdot (\epsilon_0 K \bar{E}_{in} - \epsilon_0 \bar{E}_{out}) = 0$$

$$\Phi_{in} = \Phi_{out}$$

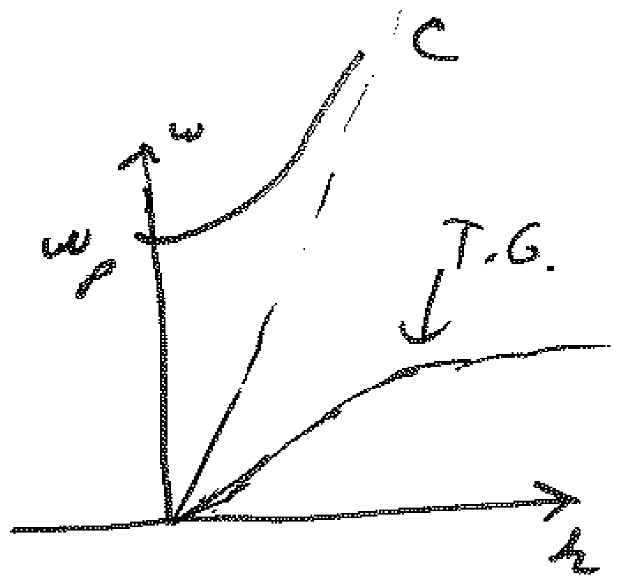

$$\nabla^2 \Phi = 0 = \frac{1}{r}\frac{\partial}{\partial r}\left(r \frac{\partial \Phi}{\partial r}\right) - h^2 \Phi = 0$$

$$\Phi(r, z, t) \propto e^{-j(\omega t - hz)}$$

$$\left.\begin{array}{ll} \Phi(r) \sim I_0(hr) & \text{INSIDE} \\ \quad\quad\;\; K_0(hr) & \text{OUTSIDE} \end{array}\right\} r = a$$

$$\left(1 - \frac{\omega_p^2}{\omega^2}\right) I_0' C_1 = K_0' C_2$$

$$I_0 C_1 = K_0 C_2$$

$$1 - \frac{\omega_p^2}{\omega^2} = \frac{I_0(ha) K_0'(ha)}{I_0'(ha) K_0(ha)}$$

VOL. 81, NO. 28 JOURNAL OF GEOPHYSICAL RESEARCH OCTOBER 1, 1976

Particle Acceleration by MHD Surface Wave and Formation of Aurora

AKIRA HASEGAWA

Bell Laboratories, Murray Hill, New Jersey 07974

Hydromagnetic surface waves, excited either by a MHD plasma instability or by an externally applied impulse, are shown to resonantly mode convert to the kinetic Alfvén wave, the Alfvén wave having a wavelength comparable to the ion gyroradius in the direction perpendicular to the magnetic field. The kinetic Alfvén wave has a component of its electric field in the direction of the ambient magnetic field and can accelerate plasma particles along the field line. Because of the property of the wave the acceleration occurs on a thin magnetic surface separated by the ion gyroradius. A possible relation between this type of acceleration and the formation of aurora arcs is discussed.

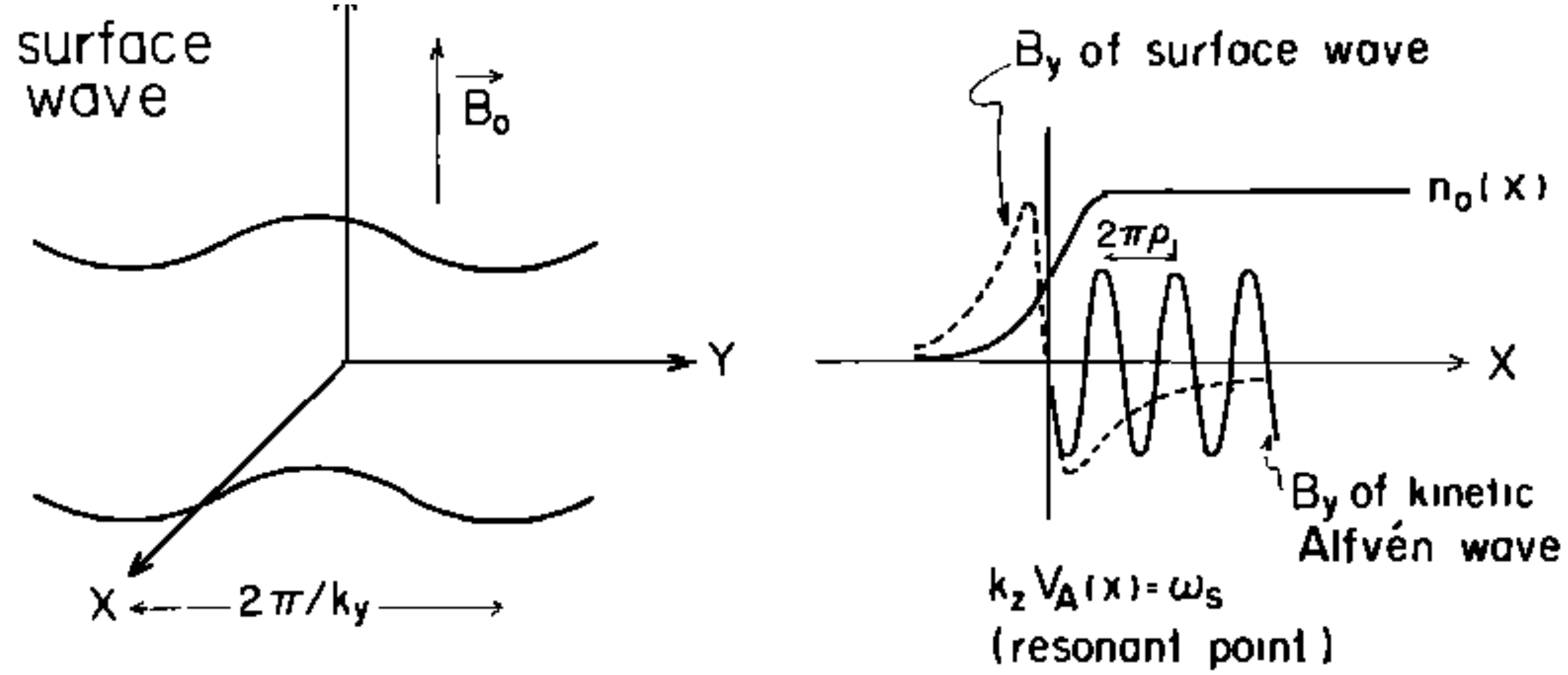

Fig. 1. Profile of the surface wave (left) and the amplitude variation of the surface and the kinetic Alfvén wave (right).

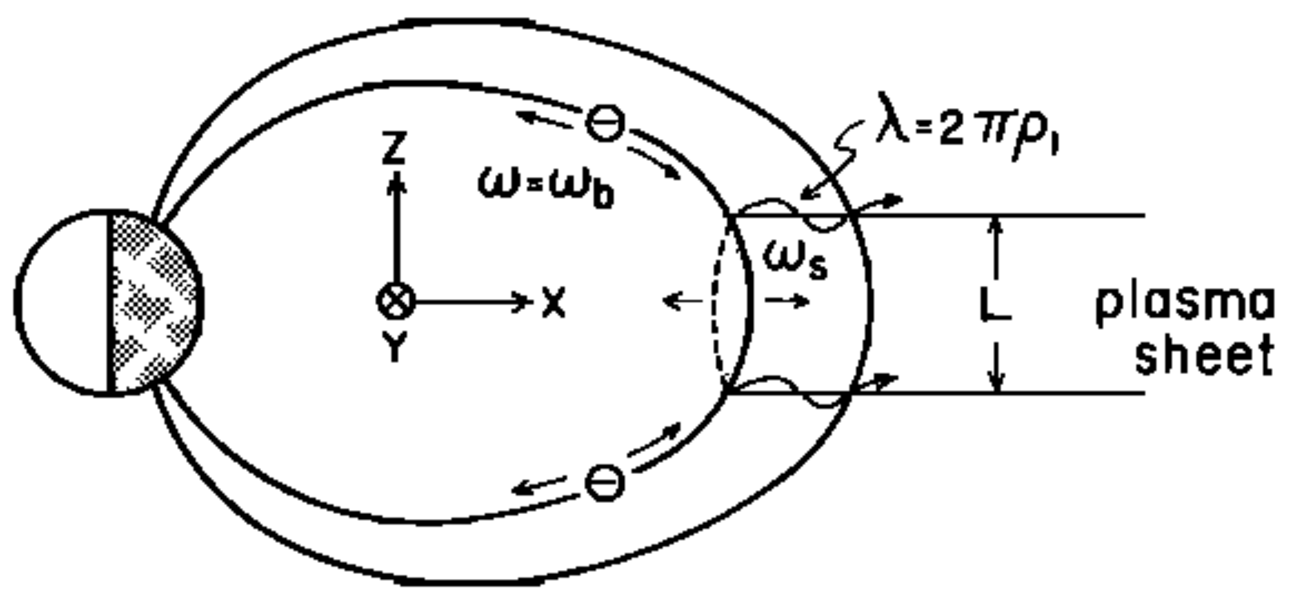

Fig. 2. The possible profile of the plasma sheet during the betatron acceleration and the bounce resonance acceleration of electrons by the kinetic Alfvén wave. The plasma sheet particles do not fill out flux tubes because the pitch angle is increased owing to the betatron acceleration.

Let us now consider a situation in which the plasma density is smoothly varying in x. In this case, $\epsilon = 1 - [\omega_p^2(x)/\omega^2]$ becomes a function of x, and hence from (2) we see that the bulk oscillation (compressible) no longer decouples from the surface wave (incompressible). Equation (2) becomes

$$\left[1 - \frac{\omega_p^2(x)}{\omega^2}\right]^{-1} \frac{\partial}{\partial x}\left[1 - \frac{\omega_p^2(x)}{\omega^2}\right]\frac{\partial \varphi}{\partial x} - k^2\varphi = 0 \qquad (7)$$

We note here that for ω corresponding to the surface wave eigenfrequency $\omega_s = \omega_p/(2)^{1/2}$ there always exists a point $x = x_0$, at which $\omega_p^2(x_0) = \omega_s^2$, because ω_p^2 is proportional to the plasma density. Near $x = x_0$ the first term in (7) dominates, and the approximate solution for φ is given by

$$\begin{aligned} \varphi &= \ln (x - x_0) & \quad x > x_0 \\ \varphi &= \ln |x - x_0| \pm i\pi & \quad x < x_0 \end{aligned} \qquad (8)$$

where a linear profile in density n_0 is assumed near $x = x_0$. The

PHYSICS OF PLASMAS **15**, 055501 (2008)

Basic physics of Alfvén instabilities driven by energetic particles in toroidally confined plasmas[a)]

W. W. Heidbrink[b)]
Department of Physics and Astronomy, University of California, I

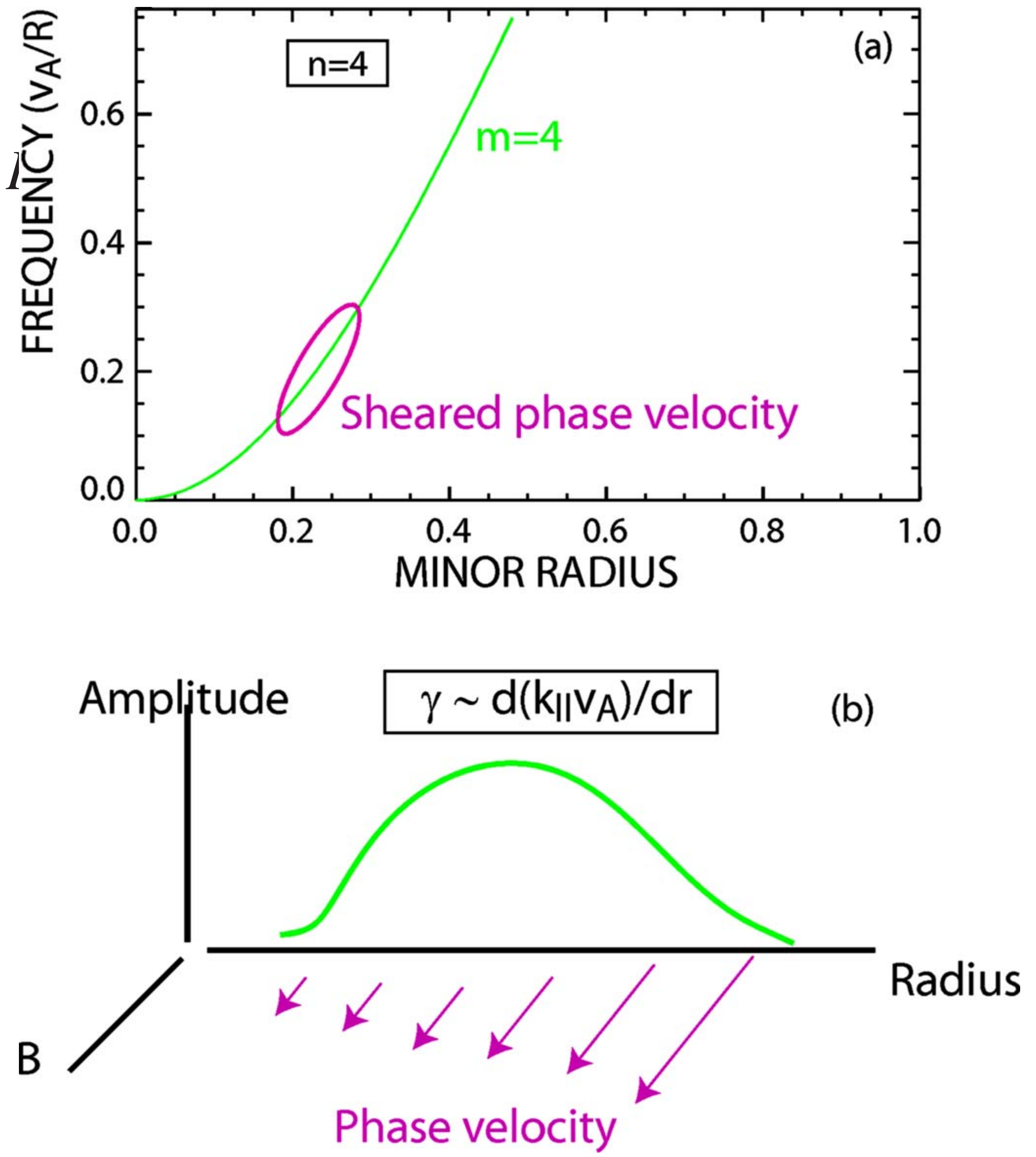

II. ALFVÉN GAP MODES

Shear Alfvén waves are transverse low frequency electromagnetic waves that propagate along the magnetic field **B**. When the wave frequency ω is small compared to the ion cyclotron frequency Ω_i and when kinetic effects are unimportant, the dispersion relation in a uniform field is simply

$$\omega = k_{\|} v_A, \tag{1}$$

$$k_{\|} = (n - mq)/R,$$

FIG. 1. (Color online) (a) Dispersion relation for an $m=4$, $n=4$ wave in a cylindrical plasma. The phase velocity is a strong function of radial position. (b) A hypothetical disturbance launched in the highlighted region. The pulse will rapidly disperse and shear.

Band Gap in a Bragg Grating

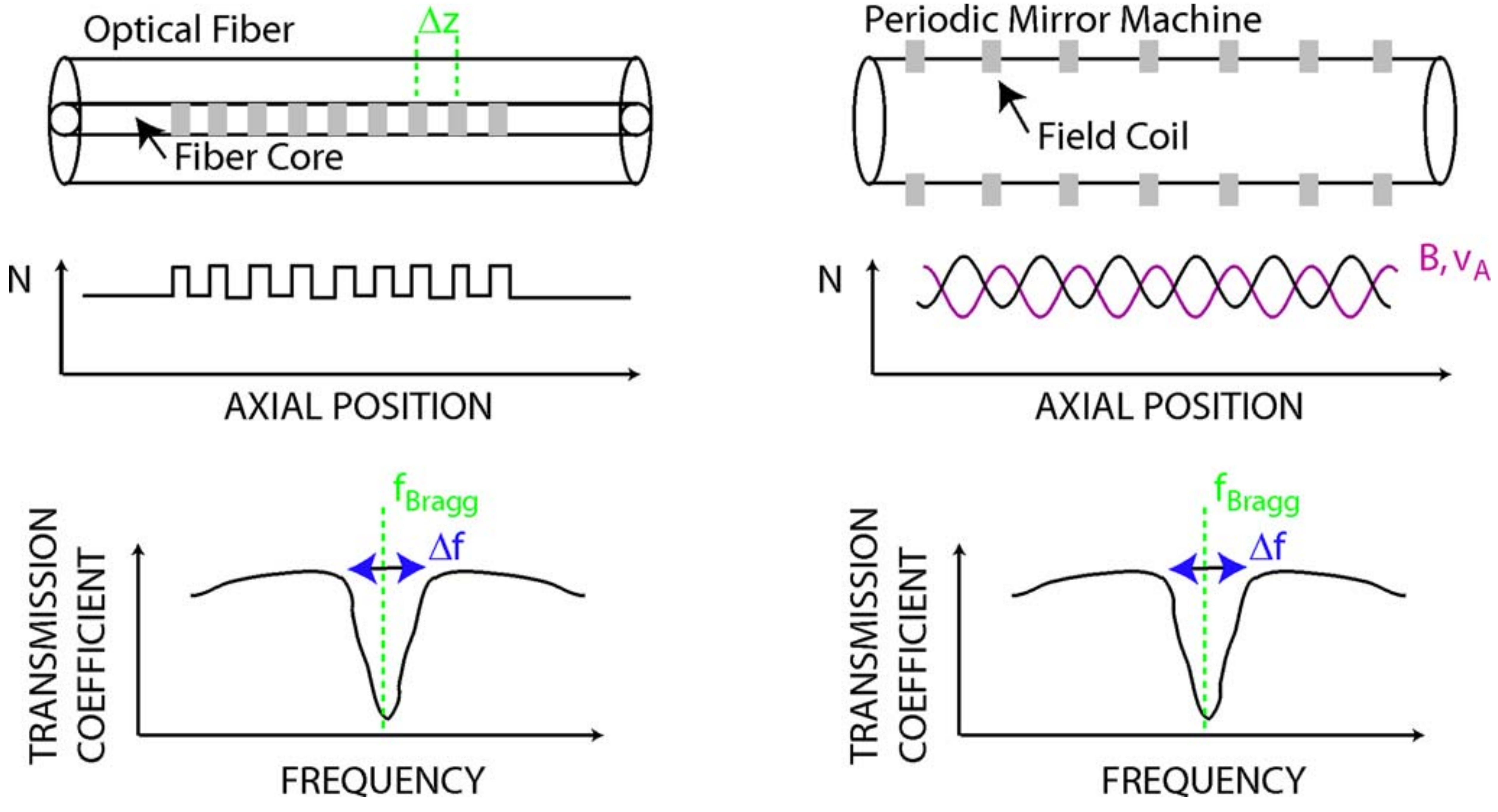

FIG. 2. (Color online) Comparison of an optical fiber with a transmission gap for visible light and a plasma with a transmission gap for shear Alfvén waves. The fiber has a periodically modulated index of refraction in its core. The plasma has a variable magnetic field that results in periodic modulation of the index of refraction N. The spatial period of the modulations is Δz. Both systems have a propagation gap at the Bragg frequency and the width of the propagation gap Δf is proportional to the amplitude of modulation of N.

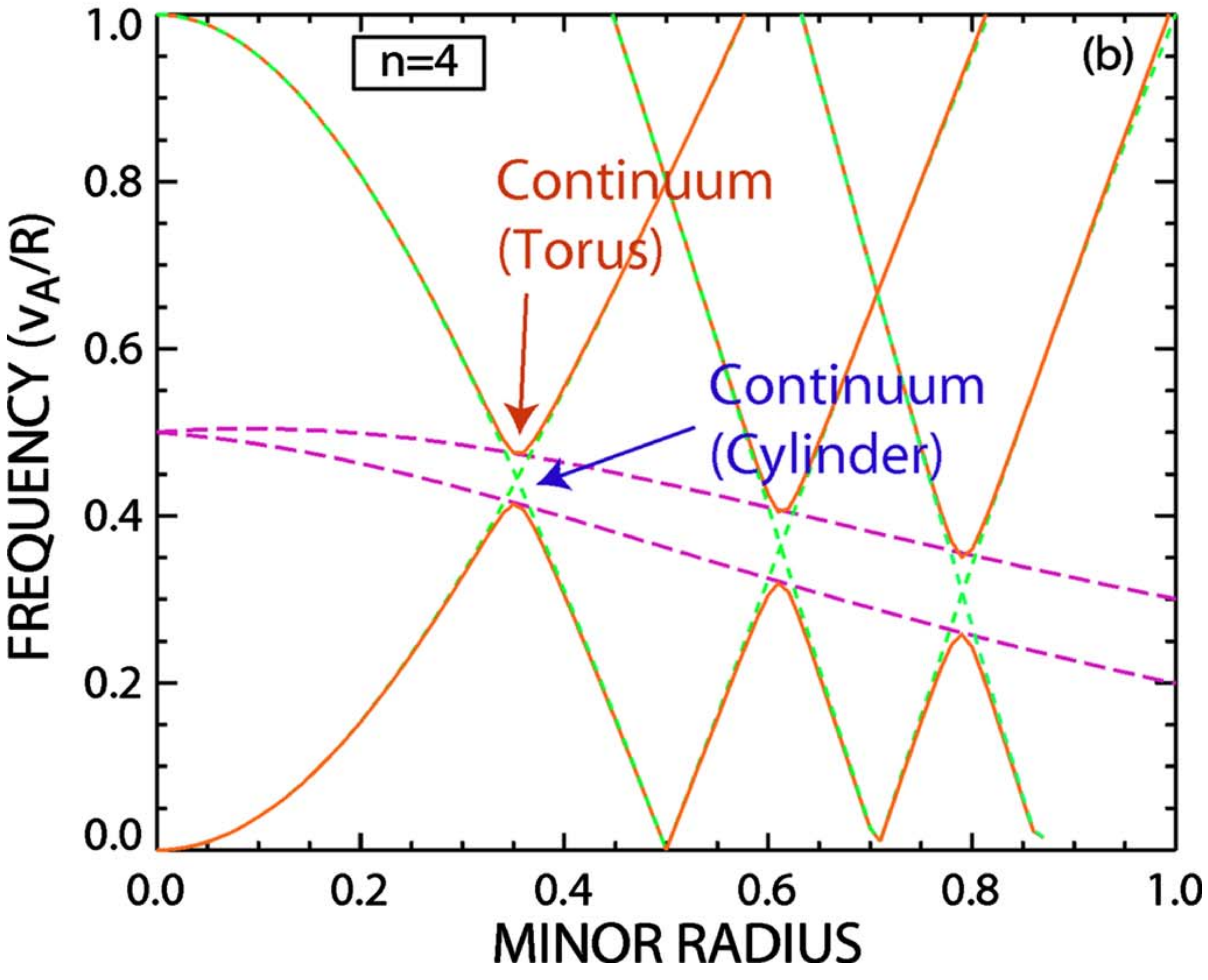

Types of Alfvén Resonances

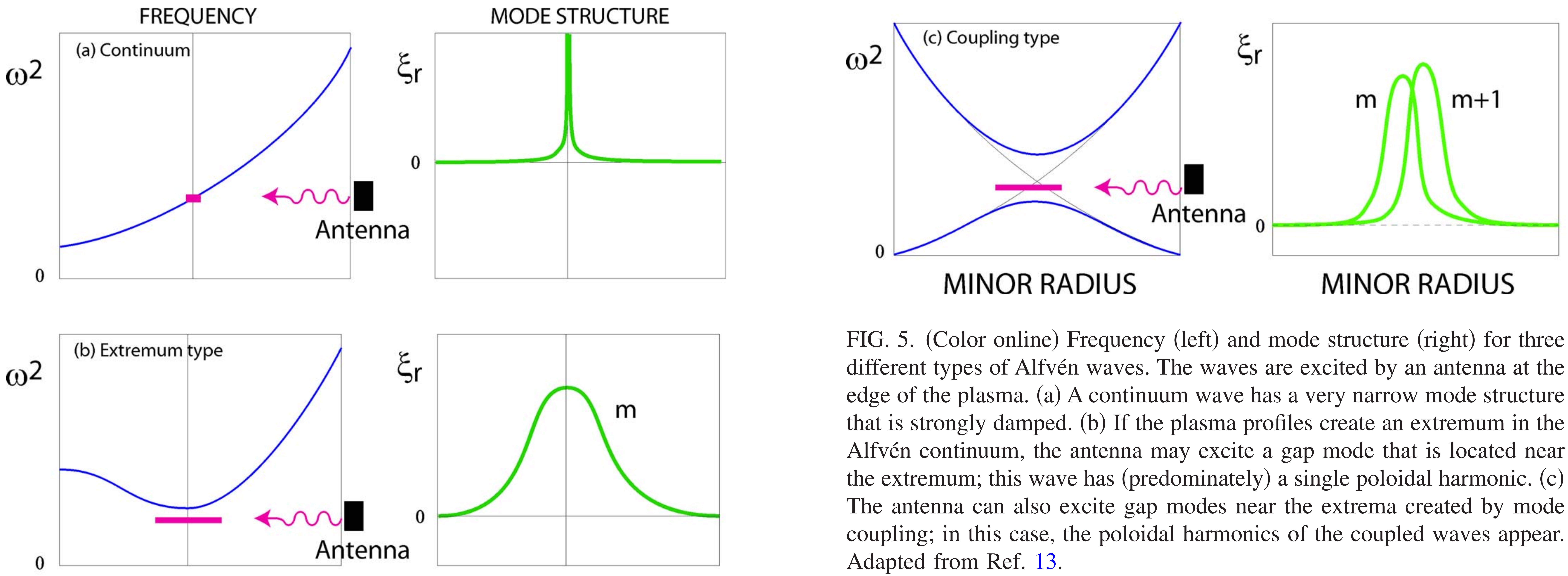

FIG. 5. (Color online) Frequency (left) and mode structure (right) for three different types of Alfvén waves. The waves are excited by an antenna at the edge of the plasma. (a) A continuum wave has a very narrow mode structure that is strongly damped. (b) If the plasma profiles create an extremum in the Alfvén continuum, the antenna may excite a gap mode that is located near the extremum; this wave has (predominately) a single poloidal harmonic. (c) The antenna can also excite gap modes near the extrema created by mode coupling; in this case, the poloidal harmonics of the coupled waves appear. Adapted from Ref. 13.

Energetic Particle Orbits

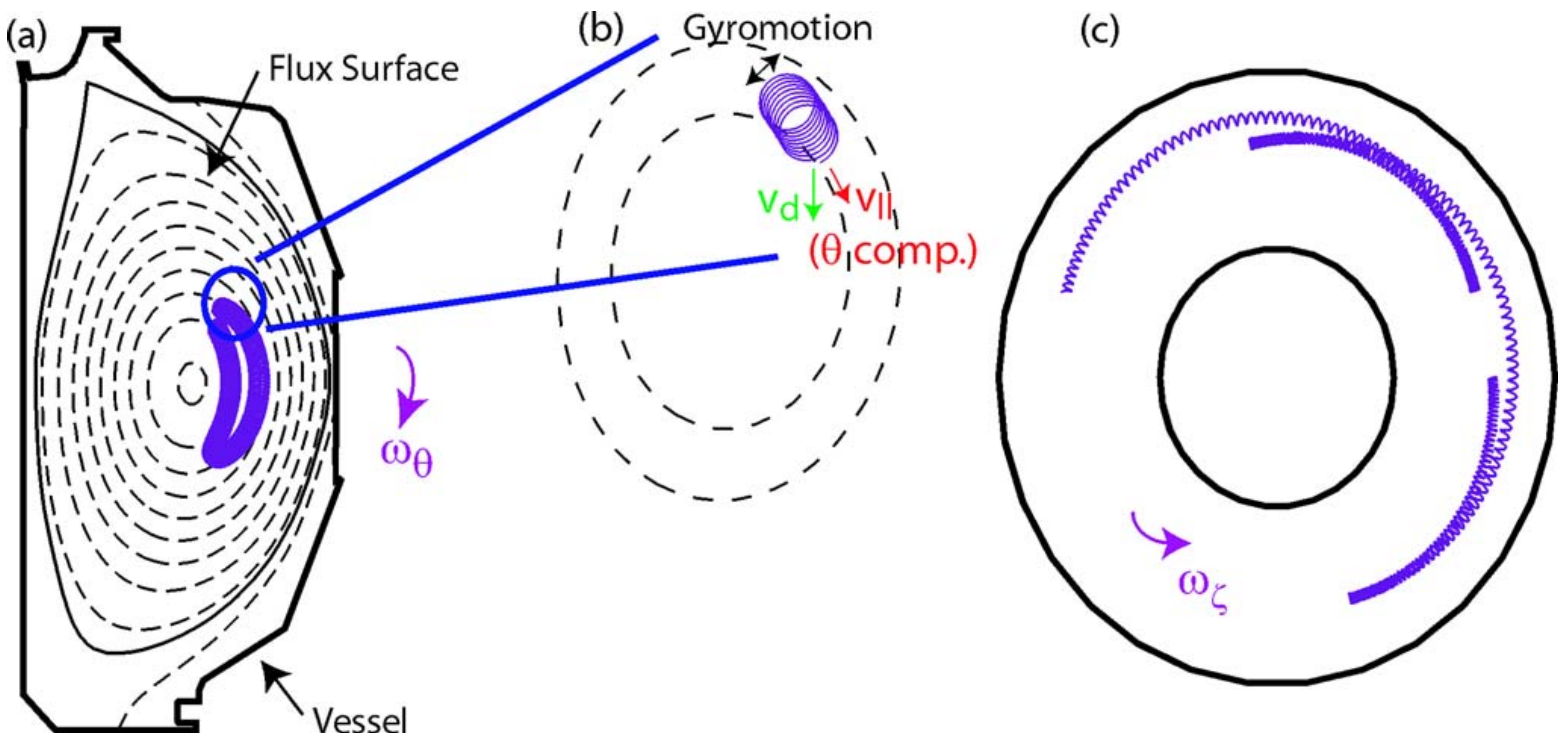

FIG. 9. (Color online) Projection of the orbit of an 80-keV deuterium beam ion in the DIII-D tokamak. (a) Elevation. The dashed lines represent the magnetic flux surfaces. The particle orbits poloidally with a frequency ω_θ. (b) Detail of the beginning of the orbit. The rapid gyromotion, parallel drift along the flux surface, and vertical drift velocity are indicated. (c) Plan view of the orbit. The particle precesses toroidally with a frequency ω_ζ.

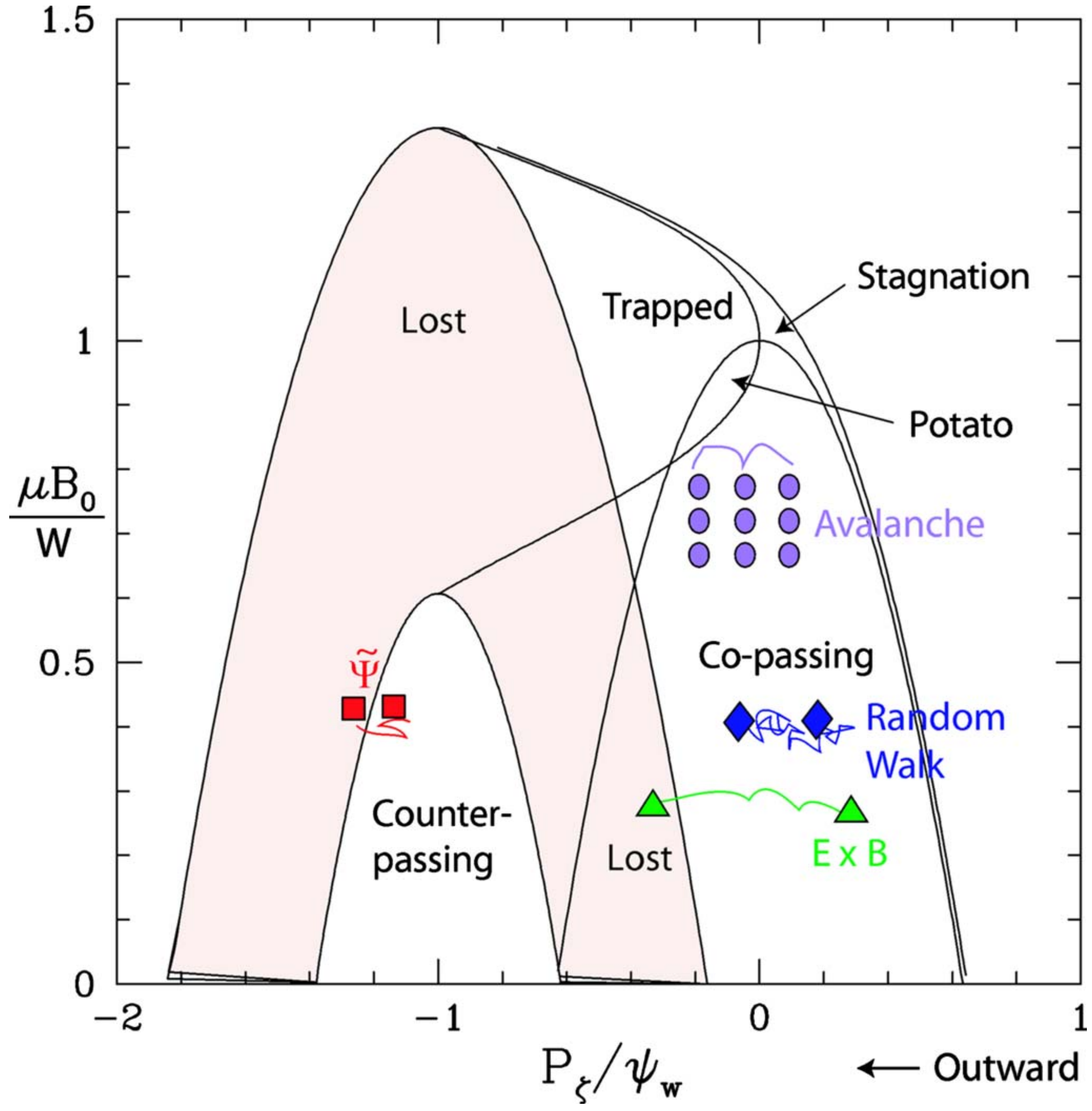

TAE-Particle Resonance

$$\omega + p\omega_\theta - n\omega_\zeta \simeq 0$$

$$\gamma \propto \omega \frac{\partial f}{\partial W} + n \frac{\partial f}{\partial P_\zeta}.$$

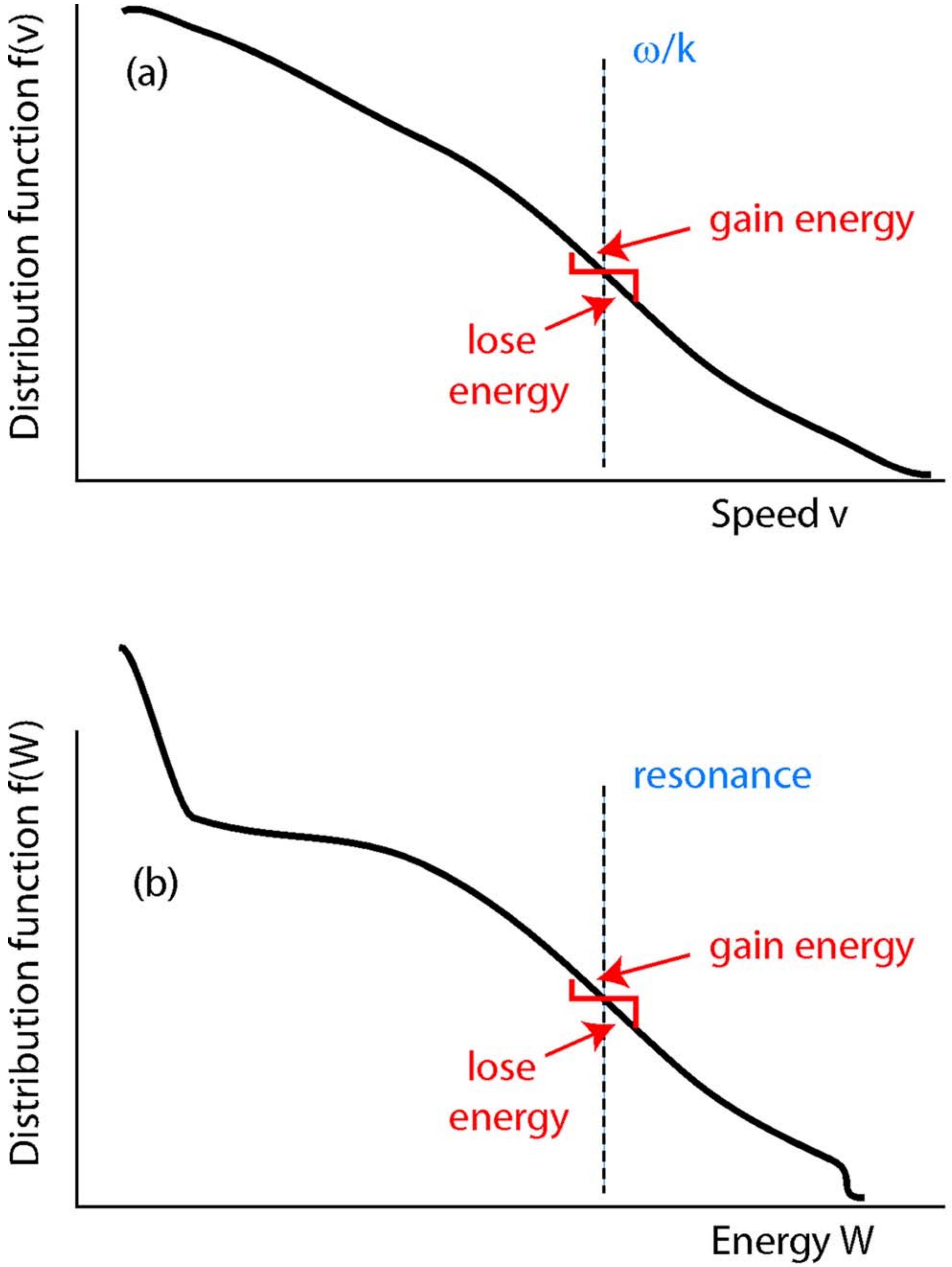

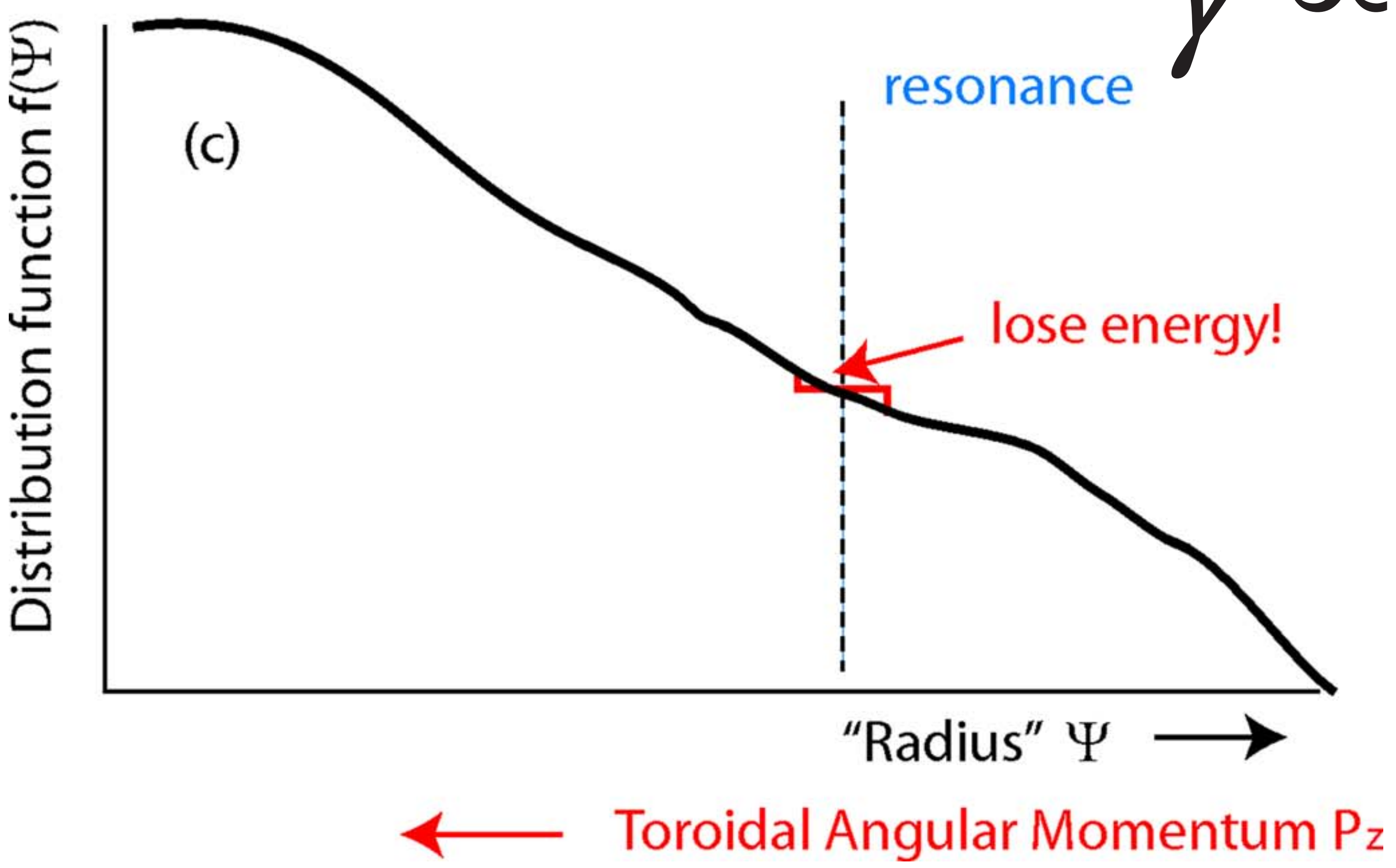

FIG. 12. (Color online) Illustration of the dependence of EP drive (or damping) on the slope of the distribution function. (a) Classic Landau damping situation: for a monotonically decreasing distribution function there are more particles that gain energy from the wave than lose energy, so the wave damps. (b) The energy distribution typically is monotonically decreasing, so the wave damps. (c) The distribution function is usually peaked on axis. The toroidal angular momentum P_ζ has the opposite dependence on radius than the flux function, so a peaked distribution function has a positive gradient $\partial f/\partial P_\zeta$ and gives net energy to the wave.

Next Class

- The structure of scientific papers…